New Developments in Semiclassical Transition State Theory

Xiao Shan, Timothy A. H. Burd, and David C. Clary*

Physical and Theoretical Chemistry Laboratory, Department of Chemistry, University of Oxford, South Parks Road, Oxford, OX1 3QZ, United Kingdom

E-mail: david.clary@chem.ox.ac.uk

Abstract

This Feature Article describes some recent developments and applications of the Semiclassical Transition State Theory (SCTST) for treating quantum tunnelling in chemical reactions. A reduced dimensional form of the SCTST is discussed and is shown to be particularly efficient as the required number of electronic structure calculations is reduced to an absolute minimum. We also describe how an alternative formulation of SCTST, called SCTST-θ, has advantages in allowing for straightforward applications of the SCTST for any form of the potential expansion at the transition state. We also illustrate the power of SCTST in applications to more complex systems. We show how polyatomic modes such as internal rotations and torsions can be treated efficiently in SCTST calculations. We also describe some applications of the method to hydrogen atom tunneling in unimolecular reactions including the degradation of chemical nerve agents and the decay of the atmospherically important Criegee intermediates.

1. Introduction

The development of efficient and reliable methods for calculating rate constants of chemical reactions is a very active area of theoretical chemistry.[1,2] Transition state theory is very widely used and can be applied directly and automatically from modern electronic structure computer packages.[3] However, this theory in its simplest form neglects quantum tunneling effects and these can be significant for reactions involving the abstraction or exchange of hydrogen atoms. Therefore, developing reaction rate theories that treat tunnelling continues to receive much attention.[4]

The most complete theory that incorporates tunnelling is quantum reactive scattering (QRS) in full dimensions using an accurate potential energy surface obtained from *ab initio* quantum chemistry calculations.[5,6] This theory can be applied using time-dependent or time-independent quantum dynamics. However, the computational cost rises exponentially with the increase of dimensionality and this currently limits the general applicability of the

full approach to reactions involving six atoms or fewer. Such calculations, however, do serve as a very useful benchmark to test the accuracy of more approximate theories.[5] Theories based on transition state theory with tunnelling corrections have been very effectively applied to many reaction problems.[3,7] However, the accuracy of such approaches can in some cases be uncertain. Other promising methods include Ring Polymer Molecular Dynamics (RPMD),[8] which exploits path integrals and involves a relatively minor adaptation of commonly used molecular dynamics codes to treat quantum effects, and the Instanton approach, which enables the calculation of tunnelling through a single periodic orbit in the reaction configuration space.[9]

Since chemical reaction rates depend exponentially on the activation energy through the Arrhenius relation, an electronic structure calculation of the highest accuracy is required to compute the height of reaction barriers.[10] This means that, despite considerable recent progress,[11] few global potential energy surfaces have the required accuracy for reactions of larger polyatomic molecules. This limits the general applicability of most of the theories described above for treating quantum tunnelling.

Semiclassical Transition State Theory (SCTST) is a computationally inexpensive method for calculating rate constants which includes the treatment of tunnelling.[12–14] The method has the distinct advantage that a global potential energy surface in all degrees of freedom from reactants to products is not needed. Instead all that is required is an expansion of the force-field around the transition state. The tunnelling probabilities are obtained from simple analytical formulae in the harmonic and anharmonic force constants which can be obtained directly from ab initio electronic structure calculations.[14] This theory was developed by Miller and co-workers in the 1990s[12?,13] but its accuracy was not clear at that time due to the small number of accurate benchmark quantum dynamics calculations that were available. It has become clear more recently that this theory can give very reliable results for quantum tunnelling[14–17] and hence SCTST has emerged as a very powerful and direct approach for computing rate constants.

Reduced dimensionality (RD) methods make quantum dynamics calculations more cost effective and applicable.[18] A general form of RD theory that we have developed and tested involves treating the chemical bonds being broken or formed using explicit quantum dynamics while the effect of the spectator vibrational modes are considered by including their harmonic frequencies in the potential energy surface.[19–23] This combined reduced dimensional and quantum chemistry (RDQC) approach has been applied to many reactions of polyatomic molecules.[4] It requires only a minimal number of accurate quantum chemistry computations and the quantum dynamics calculations are very inexpensive to carry out. The approach has been used to test the accuracy of the SCTST for the same potential energy surfaces for a range of hydrogen atom transfer reactions of polyatomic molecules and the agreement between the two sets of results is excellent in every case.[4,16,17] Combining the RD approach with SCTST also produces a highly efficient theory that will be applicable to a very wide range of reactions of larger polyatomic molecules.[24]

In this Feature Article we describe recent developments in the SCTST with particular emphasis on its application within the RD approach. Computations on a range of bimolecular and unimolecular chemical reactions are described. A short theoretical background overview of the original form of the SCTST, and examples of its applications to chemical reactions in both full-dimensions (FD) and one-dimension (1D), is given in Section 2. In Section 3, we consider the SCTST in the barrier penetration integral domain which introduces some novel features to the approach. In addition, implementation of SCTST with deep tunneling corrections and fourth order vibrational perturbation theory within the RD framework is also included for both bimolecular and unimolecular reactions. In Section 4, we discuss the latest applications and developments of the RD-SCTST including corrections to the 1D SCTST and the applications to corner-cutting heavy-light-heavy systems. Conclusions are given in Section 5 where we emphasise that SCTST has considerable potential for the efficient calculation of reliable rate constants for a wide variety of chemical reactions.

2. Theoretical Background

2.1. TST

In a standard transition state theory (TST) calculation, the rate constant is given by

$$k_{\mathrm{TST}}(T) = \frac{1}{h\beta}\frac{Q^{\ddagger}(T)}{Q^{\mathrm{R}}(T)}\exp(-\beta\Delta V_f^{\circ}), \tag{1}$$

where $\beta = k_{\mathrm{B}}^{-1}T^{-1}$, ΔV_f° is the adiabatic reaction barrier in the forward direction and $Q^{\ddagger}(T)$ and $Q^{\mathrm{R}}(T)$ are the total partition functions of the transition state and reactant, respectively. In the computation of these two total partition functions, the vibrational motions are often treated using a harmonic oscillator model. It is also possible to compute the rate constant using more accurate anharmonic vibrational partition functions. Eq. 1 can then be written as

$$k_{\mathrm{TST,anh}}(T) = \frac{1}{h\beta}\frac{Q^{\ddagger}_{\mathrm{anh}}(T)}{Q^{\mathrm{R}}_{\mathrm{anh}}(T)}\exp(-\beta\Delta V_f^{\circ}). \tag{2}$$

It should be noted that for most reactions, this error introduced by the harmonic oscillator model is negligible because of the cancellation of errors when calculating the ratio between the TS and reactant partition functions, $Q^{\ddagger}_{\mathrm{vib}}/Q^{\mathrm{R}}_{\mathrm{vib}}$. In order to achieve this cancellation of errors, one needs to use the same vibrational model for the reactant and TS. In other words, we have

$$\frac{Q^{\ddagger}_{\mathrm{vib,anh}}}{Q^{\mathrm{R}}_{\mathrm{vib,anh}}} \simeq \frac{Q^{\ddagger}_{\mathrm{vib,HO}}}{Q^{\mathrm{R}}_{\mathrm{vib,HO}}} \neq \frac{Q^{\ddagger}_{\mathrm{vib,anh}}}{Q^{\mathrm{R}}_{\mathrm{vib,HO}}} \text{ or } \frac{Q^{\ddagger}_{\mathrm{vib,HO}}}{Q^{\mathrm{R}}_{\mathrm{vib,anh}}}. \tag{3}$$

It is then easy to see that $k_{\mathrm{TST}}(T) \simeq k_{\mathrm{TST,anh}}(T)$. In addition, it is often very expensive to conduct anharmonic analyses for polyatomic molecules, thus the most commonly used TST rate constant calculation follows Eq. 1.

A common misconception is that all semiclassical transition state theory (SCTST) models are improvements to the standard TST given in Eq. 1. In reality, however, only one-dimensional (1D) SCTST is based on Eq. 1, while the full-dimensional (FD) SCTST is

based on the anharmonic TST in Eq. 2. The multi-dimensional or reduced-dimensional (RD) SCTST lies somewhere between the two. Details of the treatment and challenges of RD SCTST can be found in Section 4. Here we discuss the FD SCTST and 1D SCTST.

2.1. FD SCTST

In a FD SCTST calculation, the reaction rate constant is given by[12–14,25–27]

$$k_{\mathrm{SCTST}}(T) = \frac{1}{h}\frac{Q^{\ddagger\prime}(T)}{Q^{\mathrm{R}}_{\mathrm{anh}}(T)}\int_{E_{\mathrm{thresh}}}^{\infty} N_{\mathrm{FD}}(E_v)\exp(-\beta E_v)\mathrm{d}E_v, \tag{4}$$

where $Q^{\ddagger\prime}(T)$ is the partition function of the TS consisting of the electronic, rotational, and translational partition function. Here, $N_{\mathrm{FD}}(E_v)$ is the cumulative reaction probability (CRP). It is calculated by summing over the TS vibrational configuration dependent reaction probability,

$$N_{\mathrm{FD}}(E_v) = \sum_{\{n^{\ddagger}\}} P_{\{n^{\ddagger}\}}(E_v). \tag{5}$$

Here, $\{n^{\ddagger}\}$ corresponds to the set of quantum numbers of the non-reactive (bound) vibrational states. Each unique set is referred to as a TS vibrational configuration. Combining these two equations, we have

$$k_{\mathrm{SCTST}}(T) = \frac{1}{h}\frac{Q^{\ddagger\prime}(T)}{Q^{\mathrm{R}}_{\mathrm{anh}}(T)}\sum_{\{n^{\ddagger}\}}\int_{E_{\mathrm{thresh}}}^{\infty} P_{\{n^{\ddagger}\}}(E_v)\exp(-\beta E_v)\mathrm{d}E_v. \tag{6}$$

It should also be noted that if quantum tunneling effects were not included in the computation of $P_{\{n^{\ddagger}\}}$, then Eq. 6 would reduces to Eq. 2. In SCTST, the WKB wavefunction is used to calculate $P_{\{n^{\ddagger}\}}$, it is given by[12,13,25,26]

$$P_{\{n^{\ddagger}\}}(E_v) = \{1 + \exp[2\theta_{\{n^{\ddagger}\}}(E_v)]\}^{-1}\ , \tag{7}$$

where θ is the barrier penetration integral given by

$$\theta_{\{n^\ddagger\}}(E_v) = \frac{1}{\hbar}\int [V_{\{n^\ddagger\}}(q) - E_v]^{1/2} \mathrm{d}q$$

We now consider a TS that consists of F vibrational modes where the F-th mode is the reaction mode with an imaginary vibrational frequency. In the SCTST developed by Miller *et al.*,[12] in order to determine an analytical expression for θ in terms of easily calculable quantities, the Bohr-Sommerfeld theory is used. The reaction mode, or F-th, action variable is given by

$$2\pi\hbar(n_F + 1/2) = \oint p_F \mathrm{d}q_F = 2\int p_F \mathrm{d}q_F, \tag{8}$$

where p_F is the momentum conjugate to position q_F. For a particular TS vibrational configuration, $\{n^\ddagger\}$, it can be written as

$$p_F = [E_v - V_{\{n^\ddagger\}}(q_F)]^{1/2}. \tag{9}$$

Combining these two equations, we get

$$\frac{\pi(n_F + 1/2)}{i} = \frac{1}{\hbar}\int [V_{\{n^\ddagger\}}(q_F) - E_v]^{1/2} \mathrm{d}q_F, \tag{10}$$

where the right side of this equation is equivalent to a barrier penetration integral, $\theta_{\{n^\ddagger\}}$. We thus have

$$\frac{(n_F + 1/2)}{i} = \frac{\theta_{\{n^\ddagger\}}(E_v)}{\pi} \tag{11}$$

Perturbation theory can then be used to connect $(n_F + 1/2)$ to the energy of an incoming wavepacket. Second order vibrational perturbation theory (VPT2)[26] gives the potential

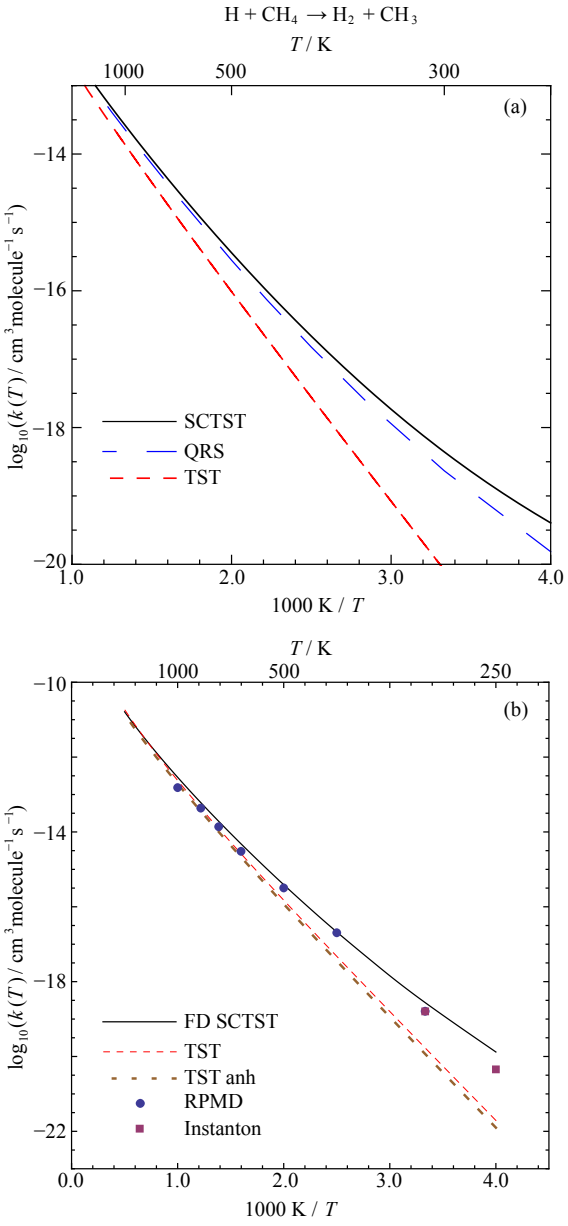

Figure 1: Application of SCTST to the H + CH_4 → H_2 + CH_3 reaction. (a) Arrhenius plot of the rate constants calculated using SCTST based on 2D PES,[28] comparing to the quantum reactive scattering (QRS) results based on the same surface. (b) Arrhenius plot of the rate constants calculated using FD SCTST, standard TST, and anharmonic TST, comparing to RPMD[29] and Instanton[30] results.

energy at the TS as:

$$E_v(n^\ddagger,\theta) = \Delta V_f + G_0 + \sum_{j=1}^{F-1}\hbar\omega_j(n_j+1/2) + \sum_{j=1}^{F-1}\sum_{k=j}^{F-1}x_{jk}(n_j+1/2)(n_k+1/2) - [\frac{\hbar\omega_F}{i} + \sum_{j=1}^{F-1}\frac{x_{jF}}{i}(n_j+1/2)][\frac{(n_F+1/2)}{i}] - x_{FF}[\frac{(n_F+1/2)}{i}]^2. \quad (12)$$

Substituting Eq. 11 into Eq. 12 and solving for θ gives

$$\theta_{\{n^\ddagger\}}(E_v) = \frac{\pi(-\Omega_{\{n^\ddagger\}} + [\Omega^2_{\{n^\ddagger\}} + 4x_{FF}(\Delta V_{f(\mathrm{anh}),\,\{n^\ddagger\}} - E_v)]^{1/2})}{2x_{FF}}, \quad (13)$$

where

$$\Omega_{\{n^\ddagger\}} = \frac{\hbar\omega_F}{i} + \sum_{i=1}^{F-1}\frac{x_{iF}}{i}(n_i+1/2), \quad (14)$$

$$\Delta V_{f(\mathrm{anh}),\,\{n^\ddagger\}} = \Delta V_f + G_0 + \sum_{j=1}^{F-1}\hbar\omega_j(n_j+1/2) + \sum_{j=1}^{F-1}\sum_{k=j}^{F-1}x_{jk}(n_j+1/2)(n_k+1/2), \quad (15)$$

where the ω_F is the reaction mode vibrational frequency and x_{jk} are the anharmonic constants. Note that in Eq. 15, the forward reaction barrier, ΔV_f, does not include the zero point energy corrections and is different from ΔV_f° in Eqs. 1 and 2. The third and fourth order derivatives of the potential energy surface (PES) with respect to the vibrational normal modes are required to calculate x_{jk} using VPT2.[14,26,27,31,32] Detailed VPT2 derivations can be found in Refs. 26,31. These higher order derivatives can be obtained from an analytically fitted PES[17,24] or from *ab initio* calculations.[14,15,27,33]

We use the H + CH_4 → H_2 + CH_3 reaction to illustrate the application of SCTST to a real chemical reaction. The results are shown in Fig. 1. In Fig. 1(a), the higher order derivatives were obtained from a two-dimensional analytical PES.[17,28] The analytical PES function was fitted to *ab initio* energies calculated at CCSD(T)//MP2/cc-pVTZ level for grid points along two active vibrational modes.[28] The SCTST result (black curve) shows good agreement compared to the rate constant from a quantum reactive scattering (QRS)

calculation (dashed blue curve) performed on the same PES.

In Fig. 1(b), the SCTST results were calculated directly from *ab initio* calculations at CCSD(T)//MP2/aug-cc-pVTZ level. Comparing the standard TST (dashed red curve) and the anharmonic TST (dashed brown curve), we can see the relationship given in Eq. 3 stands. The FD SCTST rate constant converges to the TST results at high temperature. The quantum tunneling contribution becomes more pronounced at temperatures typically lower than 500K. We can also see that FD SCTST has an excellent agreement when compared to other theoretical results[29,30] at these temperatures.

2.2. 1D SCTST

The FD SCTST has two major sources of computational costs. The computation of the third and fourth order derivatives of the PES can quickly become exceedingly expensive as the size of system increases.[14,27,32] In addition, the calculation of the cumulative reaction probability via Eq. 5 is also a formidable task, because the number of TS configurations, $\{n^{\ddagger}\}$, increases exponentially with the number of degrees of freedom. Enumeration of all possible configurations for even 3 or 4 degrees of freedom is very computationally expensive.[33] For larger systems, one can use the Wang-Landau algorithm[34–36] and its implementation for parallel architectures[37] to obtain an approximate density of states and tunneling probability. Generally speaking, even with these methods, the FD SCTST can quickly become too expensive when studying relatively large systems. It is therefore desirable to develop an approximate method based on the principle of SCTST, but scales better with system size. We first discuss here the one-dimensional approach, which has been applied to various reactions, including H abstractions,[24,32,38] H exchange,[39] and unimolecular H transfers.[40,41] In Section 4, we shall explain the limitation of this method and suggest possible solutions.

To simplify the FD SCTST expression of rate constants in Eq. 6 into the 1D SCTST equation, three approximations are made. Firstly, the reaction mode is assumed to be decoupled from the other bound vibrational modes. This allows the separation of the summation

in CRP calculation from the integration over energy in the rate constant calculation. We have

$$k(T) = \frac{1}{h}\frac{Q^{\ddagger}_{\mathrm{anh}}(T)}{Q^{\mathrm{R}}_{\mathrm{anh}}(T)}\int_{E_{\mathrm{thresh}}}^{\infty} P_{\{0\}}(E_v)\exp(-\beta E_v)\mathrm{d}E_v. \tag{16}$$

Here the CRP is replaced by the ground state reaction probability, $P_{\{0\}}(E_v)$ and the total partition function of the TS, $Q^{\ddagger}_{\mathrm{anh}}(T)$ now includes the anharmonic vibrational partition functions for all the bound modes.

The second assumption utilises the relationship given in Eq. 3 that we assume all the bound vibrational modes in both TS and reactants can be treated harmonically. The rate constants equation can then be written as

$$k(T) = \frac{1}{h}\frac{Q^{\ddagger}(T)}{Q^{\mathrm{R}}(T)}\int_{E_{\mathrm{thresh}}}^{\infty} P_{\{0\}}(E_v)\exp(-\beta E_v)\mathrm{d}E_v. \tag{17}$$

It should be noted that in the calculation of $P_{\{0\}}$, the harmonic ground state energies are used. Following Eqs. 13 to 15 and the approximations given so far, x_{FF} and G_0 are the two required parameters to compute this rate constant. In a FD VPT2 calculation, they are given by

$$x_{FF} = \frac{\hbar}{16\omega_F^2}(f_{FFFF} - \sum_{i=1}^{F}\frac{f_{FFi}^2}{\omega_i^2}\frac{8\omega_F^2 - 3\omega_i^2}{4\omega_F^2 - \omega_i^2}), \tag{18}$$

and

$$\begin{aligned} G_0 \;=\; & \frac{\hbar}{64}\frac{f_{FFFF}}{\omega_F^2} - \frac{7\hbar^2}{576}\frac{f_{FFF}^2}{\omega_F^4} + \frac{3\hbar^2}{64}\sum_{i\neq F}\frac{f_{iiF}^2}{(4\omega_i^2 - \omega_F^2)\omega_i^2} \\ & -\frac{\hbar^2}{4}\sum_{i<j<F}\frac{f_{ijF}^2}{[(\omega_i+\omega_F)^2 - \omega_j^2][(\omega_i - \omega_F)^2 - \omega_j^2]}, \end{aligned} \tag{19}$$

where f_{FFF} andf_{FFFF} is the third and fourth order derivative of the PES with respect to the reaction mode, respectively. f_{iiF} and f_{ijF} are the coupling third order derivatives between the reaction mode and bound modes. The computation of these derivatives using *ab initio* calculations can still be considerably expensive.

To further reduce the computational cost of the calculation, in the final approximation of 1D SCTST, we assume that all coupling terms in the third order derivatives are 0 between the reaction mode and the bound modes. Therefore, in 1D SCTST, we have

$$x_{FF}^{1D} = \frac{\hbar}{16\omega_F^2}(f_{FFFF} - \frac{5f_{FFF}}{3\omega_F^4}), \tag{20}$$

and

$$G_0^{1D} = \frac{\hbar}{64}\frac{f_{FFFF}}{\omega_F^2} - \frac{7\hbar^2}{576}\frac{f_{FFF}^2}{\omega_F^4}. \tag{21}$$

Now, it is clear to see that all the additional cost of a 1D SCTST to a standard TST is the computation of f_{FFF} and f_{FFFF}, which can be easily done using numerical differentiation of single point energies at geometries displaced along the reaction mode. At a minimum, only four single point energies are required, in addition to a standard TST calculation.

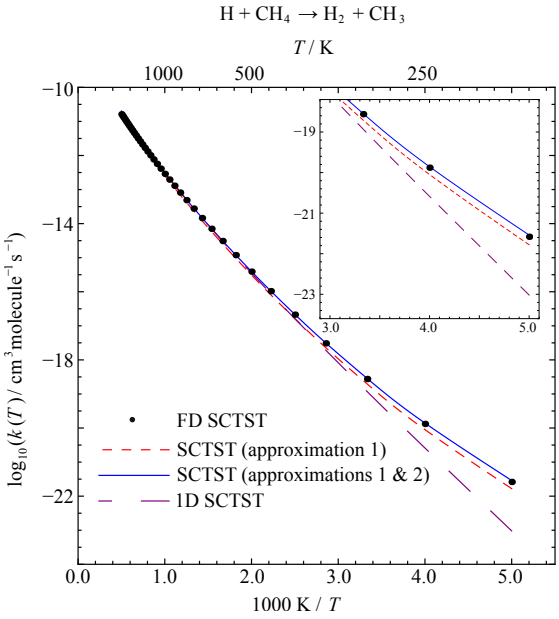

Figure 2: Application of FD SCTST and approximated SCTST to the H + CH_4 → H_2 + CH_3 reaction.

We show, in Fig. 2, the rate constants for the H + CH_4 → H_2 + CH_3 reaction calculated using the different level of approximations discussed here. It can be seen that the rate constants calculated after the first two levels of approximations show very good agreement

to the FD SCTST results. The simplest form of 1D SCTST agrees well with the FD SCTST for temperatures above 300K, but underestimates the rate as temperature decreases.

2.3. Deep tunneling

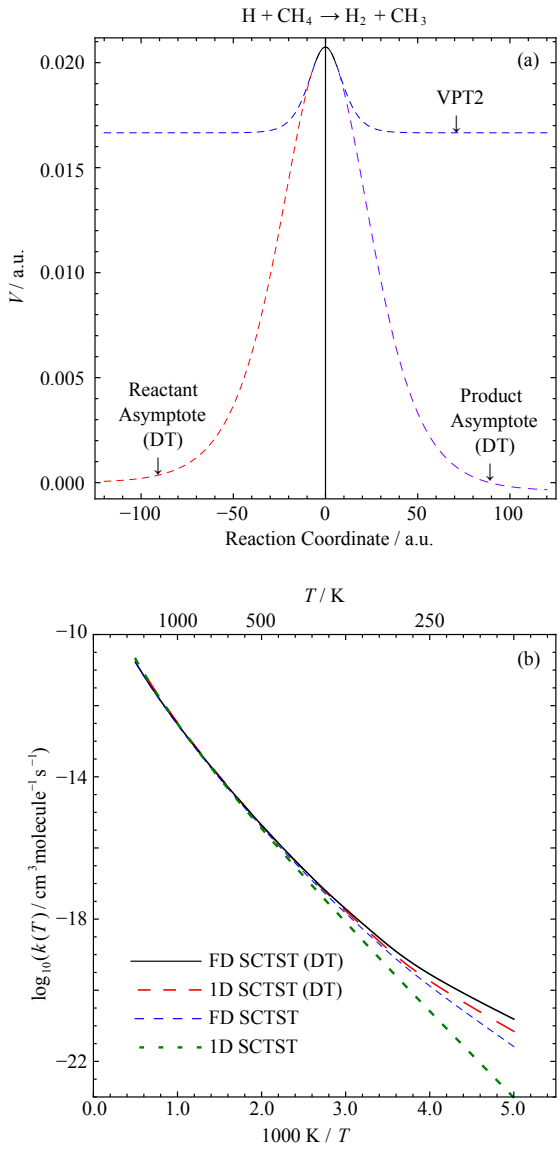

Figure 3: DT corrections to the SCTST calculations for the $H + CH_4 \rightarrow H_2 + CH_3$ reaction. (a) the comparison between DT corrected barrier and VPT2 barrier, (b) the comparison between the DT corrected FD and 1D SCTST rate constants.

In reaction rate constant studies, deep tunneling refers to reactions proceeding at energies well below the barrier height. At 200K, the simplest 1D SCTST typically underestimates the

rate constant by ~ 30 times when compared to the FD SCTST. This underestimation is a result of the VPT2 expansion of the potential around the TS being inaccurate in the reactant and product asymptotic regions. This problem has been discussed in great detail in Ref. 42. A solution given by Wagner *et al.*[42] is referred to as the deep tunneling (DT) correction to the SCTST in the current work. In the DT correction, the reaction potential is approximated by a piecewise continuous function comprised of three asymmetric Eckart segments chosen to match the forward and reverse barrier heights, the reaction mode frequency and anharmonic constant. The segments are also chosen such that the barrier is continuous and smooth at all times. In order to apply the DT correction to the SCTST, the reverse barrier height of a reaction is also required[32,42] .

We show in Fig. 3(a) the 1D VPT2 barrier and the DT corrected barrier for the H + $CH_4 \rightarrow H_2$ + CH_3 reaction, the three pieces of the DT corrected barrier are marked with different colours. The rate constants with and without DT correction are shown in Fig. 3(b). The DT corrected 1D SCTST has a much better agreement with the FD SCTST at low temperatures. It is also interesting to note that the DT correction has a greater impact on the 1D calculation than the FD one.

3. Derivation of SCTST-θ

3.1. General derivation

In the previous section, we discussed the most common way of deriving SCTST as well as practical simplifications of the FD SCTST within the reduced dimensionality framework. However, this derivation can become complicated or even break down when a more accurate potential function is applied.[42–44] For example, when a VPT4 potential is used rather than the VPT2, the relationship in Eq. 13 is obtained by solution of a cubic equation in θ,[43,44] and higher orders of perturbation theory would require analytical solutions to higher order polynomials, which do no exist in general. In this section, we discuss an alternative formula-

tion of SCTST proposed by Miller and co-workers,[45] which we shall refer to as the SCTST-θ in this paper. This formulation allows for any potential $E(\theta)$ to be used and provides a more flexible and intuitive framework to view the SCTST.

In Eq. 6, the integration is performed in the energy domain. Miller and co-workers[45] suggested that the same integration can also be done in the barrier penetration integral, θ, domain. The FD SCTST is then given by

$$k_{\text{FD SCTST}-\theta}(T) = \frac{1}{h}\frac{Q^{\ddagger\prime}(T)}{Q^{\text{R}}_{\text{anh}}(T)}\sum_{\{n^\ddagger\}}\int_{\theta_\text{T}}^{-\infty}\frac{\exp[-\beta E_v(n^\ddagger,\theta)]}{1+\exp(2\theta)}\frac{\partial E_v(n^\ddagger,\theta)}{\partial\theta}\text{d}\theta, \tag{22}$$

where $E_v(n^\ddagger,\theta_\text{T}) = E_\text{thresh}$. Performing the integration by parts, we get

$$\begin{aligned}\int_{\theta_\text{T}}^{-\infty}\frac{\exp[-\beta E_v(n^\ddagger,\theta)]}{1+\exp(2\theta)}\frac{\partial E_v(n^\ddagger,\theta)}{\partial\theta}\text{d}\theta \quad &= \frac{\exp[-\beta E_v(n^\ddagger,\theta_\text{T})]}{\beta[1+\exp(2\theta_\text{T})]} + \frac{1}{\beta}\int_{-\infty}^{\theta_\text{T}}\frac{\text{sech}^2(\theta)}{2}\exp[-\beta E_v(n^\ddagger,\theta)]\text{d}\theta \\ &= \frac{\exp(-\beta E_\text{thresh})}{\beta[1+\exp(2\theta_\text{T})]} + \frac{1}{\beta}\int_{-\infty}^{\theta_\text{T}}\frac{\text{sech}^2(\theta)}{2}\exp[-\beta E_v(n^\ddagger,\theta)]\text{d}\theta.\end{aligned}$$

We note that the first term of the right hand side of the equation is the Boltzmann weighted reaction probability at energy threshold, E_thresh, which is negligible compared to the second part of the equation.[45] Eq. 22 can be reduced to

$$k_{\text{FD SCTST}-\theta}(T) = \frac{1}{h\beta}\frac{Q^{\ddagger\prime}(T)}{Q^{\text{R}}_{\text{anh}}(T)}\sum_{\{n^\ddagger\}}\int_{-\infty}^{\theta_\text{T}}\frac{\text{sech}^2(\theta)}{2}\exp[-\beta E_v(n^\ddagger,\theta)]\text{d}\theta. \tag{23}$$

In order to use Eq. 23, it is only necessary to know the potential energy as a function of θ , and no inversion is required . As shown in Eq. 12, in VPT2, $E_v(n^\ddagger,\theta)$ is given by

$$E_v(n^\ddagger,\theta) = \Delta V_{f(\text{anh}),\,\{n^\ddagger\}} - \Omega_{\{n^\ddagger\}}(\frac{\theta}{\pi}) - x_{FF}(\frac{\theta}{\pi})^2. \tag{24}$$

It should be noted that the FD SCTST rate constant given in Eqs. 23 and 24 is mathematically equivalent to the original formulation in Eq. 6, and hence it does not reduce the computational cost.

In this formulation, the 1D SCTST approximations become very easy to understand. The first two approximations simply remove the anharmonic terms apart from x_{FF} from Eq. 24, we then have

$$E_v^{\mathrm{1D}}(n^{\ddagger},\ \theta) = \Delta V_f + G_0 + \sum_{j=1}^{F-1} \hbar\omega_j(n_j + 1/2) - \frac{\hbar\omega_F}{i}(\frac{\theta}{\pi}) - x_{FF}(\frac{\theta}{\pi})^2. \tag{25}$$

Substituting this into Eq. 23 and extracting all the bound vibrational modes of TS from the integration, we get

$$\begin{aligned} k_{\mathrm{1D\ SCTST}-\theta}(T) = \frac{1}{h\beta}\frac{Q^{\ddagger\prime}(T)}{Q^{\mathrm{R}}(T)} \sum_{\{n^{\ddagger}\}} \exp\{-\beta[\Delta V_f + \sum_{j=1}^{F-1} \hbar\omega_j(n_j + 1/2)]\} \\ \times \int_{-\infty}^{\theta_{\mathrm{T}}} \frac{\mathrm{sech}^2(\theta)}{2} \exp[-\beta(G_0 - \frac{\hbar\omega_F}{i}(\frac{\theta}{\pi}) - x_{FF}(\frac{\theta}{\pi})^2)]\mathrm{d}\theta. \end{aligned} \tag{26}$$

The summation term is now simply the vibrational partition function of the TS, so the 1D SCTST rate constant equation can be written as

$$k_{\mathrm{1D\ SCTST}-\theta}(T) = k_{\mathrm{TST}}(T)\kappa_{\mathrm{1D}}(T), \tag{27}$$

where the tunneling correction, $\kappa_{\mathrm{1D}}(T)$, is given by

$$\kappa_{\mathrm{1D}}(T) = \int_{-\infty}^{\theta_{\mathrm{T}}} \frac{\mathrm{sech}^2(\theta)}{2} \exp[-\beta E^{\mathrm{anh(1D)}}(\theta)]\mathrm{d}\theta, \tag{28}$$

with

$$E^{\mathrm{anh(1D)}}(\theta) = G_0 - \frac{\hbar\omega_F}{i}(\frac{\theta}{\pi}) - x_{FF}(\frac{\theta}{\pi})^2.$$

It is clear to see that in order to carry out the 1D SCTST calculation, one only needs G_0 and x_{FF}, the acquisition of which has been discussed in Section 2.2. Note that although in Eq. 28 the tunneling is seemingly independent of the reaction barrier height, θ_{T} still must satisfy $E_v(n^{\ddagger}, \theta_{\mathrm{T}}) = E_{\mathrm{thresh}}$, for which the barrier height is required. The relationship between θ_{T}

and E_{thresh} will be discussed in detail in Section 3.2.

3.2. Parabolic Limit

In the parabolic barrier limit ($x_{FF} = 0$), Eq. 28 becomes,

$$\kappa_{\text{HO}}(T) = \int_{-\infty}^{\theta_{\text{T}}} \frac{\text{sech}^2(\theta)}{2} \exp[\frac{-i\beta\hbar\omega_F\theta}{\pi}]\text{d}\theta. \tag{29}$$

This integration can be performed analytically:

$$\begin{aligned} \int \frac{\text{sech}^2(\theta)}{2} \exp[\frac{\tau\theta}{\pi}]\text{d}\theta &= \frac{\exp(\frac{\tau\theta}{\pi})}{2(\tau+2\pi)}[-\tau\exp(2\theta)\ {}_2F_1(1, 1+\frac{\tau}{2\pi}, 2+\frac{\tau}{2\pi}; -\exp(-2\theta)) \\ &\quad +(\tau+2\pi)\ [{}_2F_1(1, \frac{\tau}{2\pi}, 1+\frac{\tau}{2\pi}; -\exp(2\theta)) + \tanh(\theta)] \end{aligned} \tag{30}$$

where $\tau = -i\beta\hbar\omega_F$ and ${}_2F_1$ is the hypergeometric function. Note that this integration is performed as indefinite integral. If the upper limit of the integration is chosen to be $+\infty$, then under the condition$0 \leq i\beta\hbar\omega_F < 2\pi$, Eq. 30 reproduces the Wigner tunneling correction,[46]

$$\kappa_{\text{HO}}(T)|_{-\infty}^{+\infty} = \kappa_{\text{W}}(T) = \frac{i\beta\hbar\omega_F/2}{\sin(i\beta\hbar\omega_F/2)}. \tag{31}$$

When $i\beta\hbar\omega_F = 2\pi$, the corresponding temperature is often referred to as the crossover temperature, T_{c}, at which the Wigner correction diverges.

It should be noted, however, for most chemical reactions, θ_{T} in Eq. 29 is not $+\infty$. To calculate θ_{T}, one can simply solve a linear function of θ based on Eq. 24 with only the harmonic terms,

$$\Delta V_f^\circ - \frac{\hbar\omega_F}{i\pi}\theta_{\text{T}} = E_{\text{thresh}}.$$

For an exothermic reaction, $E_{\text{thresh}} = 0$, while for an endothermic reaction, $E_{\text{thresh}} = \Delta V_f^\circ - \Delta V_r^\circ$. Here ΔV_r° is the adiabatic reverse barrier. Therefore, in order to compute the tunneling correction given in Eq. 29, one does not need any more *ab initio* calculations in addition to

the standard TST.

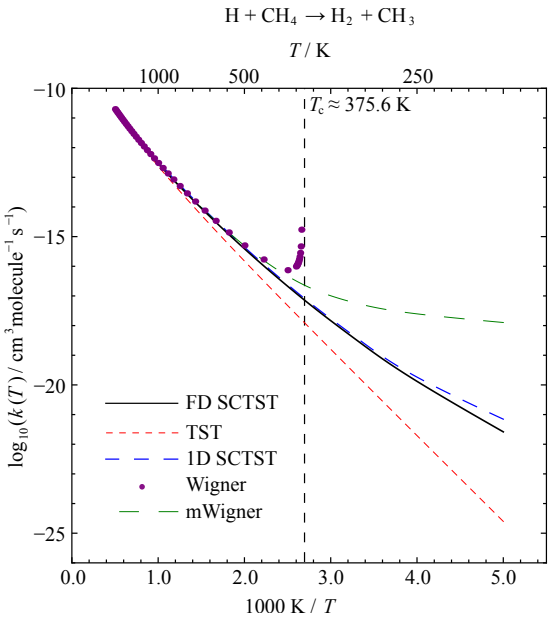

Figure 4: Comparison between Wigner, modified Wigner, 1D SCTST, FD SCTST and standard TST rate constants for the H + CH_4 → H_2 + CH_3 reaction.

A comparison between the calculated rate constants using the methods discussed so far in this work for the H + CH_4 → H_2 + CH_3 reaction is shown in Fig. 4. The reaction is exothermic, T_c is ∼ 375.6 K , and θ_T for the modified Wigner rate is ∼ 8.718. We can see that, as expected, the Wigner rate constant diverges when approaching T_c. Although the modified Wigner result (dashed green curve) continues for T below T_c, it significantly over estimates the reaction rate. This is easily understood by comparing Eq. 29 to Eq. 28. x_{FF} is negative for this reaction, which results in a smaller area under curve for the integration for the 1D SCTST than the modified Wigner. Equivalently, a negative x_{FF} leads to a wider barrier than the parabolic one.

3.2. Deep tunneling and VPT4 in the SCTST-θ

In the last section, we derived the SCTST-θ proposed by Miller and co-workers[45] and showed how to implement the 1D SCTST in this framework. We now turn our focus to the key relationship, E_v as a function of θ. The VPT2 expression is given in Eq. 24. In Fig. 5 we

graphically show an example of this for the CH_3+CH_4 reaction in the 1D approximation. VPT2 is based on a quadratic expansion of the surface about the TS, and hence is expected to be accurate for $\theta \simeq 0$, since $\theta = 0$ corresponds to the TS. The upper integration limit of the SCTST-θ formula, θ_{T}, corresponds to the minimum value of E_v, E_{min}. For $\theta > \theta_{\mathrm{T}}$, E_v is not physically meaningful. In principle, this minimum value of E_v should equal to E_{thresh}, given by

$$E_{\mathrm{thresh}} = \begin{cases} 0 & \text{for symmetric or exothermic reactions} \\ \Delta V_f - \Delta V_r & \text{for endothermic reactions} \end{cases}$$

where ΔV_r is the reverse barrier height. However, in the VPT2 calculation, E_{min} is often a poor approximation for E_{thresh}. In Fig. 5, we have $E_{\mathrm{min}} > E_{\mathrm{thresh}} = 0$. The VPT2 expression therefore ignores tunneling for $E_{\mathrm{thresh}} < E < E_{\mathrm{min}}$, and thus underestimates the rate constants significantly at low T. This problem has been identified by Wagner *et al.*[42] Numerous works[15,42–44] have been devoted to improving the SCTST in the deep tunneling regime. Here we discuss two methods and their implementation in the SCTST-θ formula.

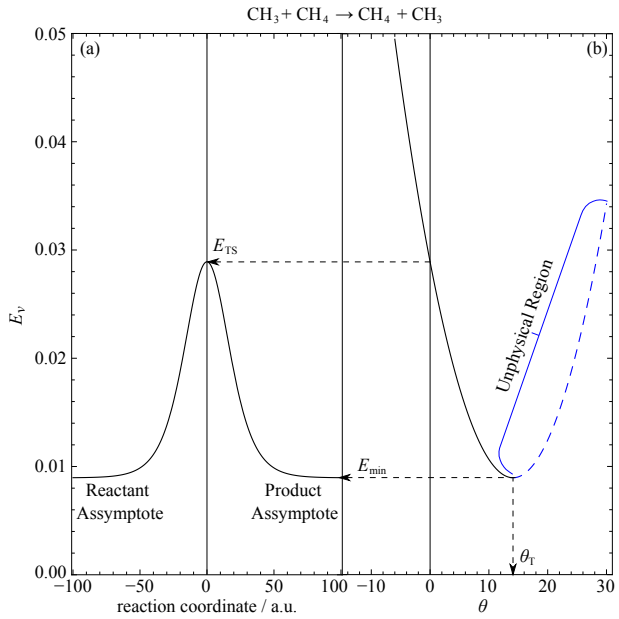

Figure 5: Plots of (a) the VPT2 barrier and (b) E_v as a function of θ for the CH_3 + $CH_4 \rightarrow CH_4$ + CH_3 reaction.

The first method is to use a higher order perturbation theory, for example VPT4. Here the energy is given by

$$E(n^{\ddagger},\theta) = V_0 + G - W\frac{\theta}{\pi} - X\left(\frac{\theta}{\pi}\right)^2 + Y\left(\frac{\theta}{\pi}\right)^3 \tag{32}$$

where V_0 is the $\{n^{\ddagger}\}$ state dependent potential barrier height, G is the anharmonic correction to the potential, and W, X, and Y are given by complex, but analytical functions of up to sixth order derivatives of the PES at the transition state, as derived by Stanton *et al.*[43] Note that in the original SCTST, Eq. 32 would need to be solved for θ, requiring inversion of a cubic equation. This is no longer necessary in SCTST-θ, and the VPT2 expression in Eq. 23 can simply be replaced with its VPT4 counterpart. Moreover, it is trivial to extend this to even higher order perturbation theories, which would not be possible in the original SCTST, owing to having to invert a quartic (or higher order polynomial) analytically. This has been shown to improve behaviour in the deep tunneling regime for the colinear H + H_2 reaction,[43] and several one-dimensional analytical potentials.[44] It is clear, however, that this approach requires significantly more *ab initio* calculations, in order to determine the fifth and sixth order derivatives of the potential. Within the one-dimensional approximation this becomes tractable, but still a significant expense.

A more efficient solution was determined by Wagner *et al.*[42] as discussed in section 2.3. This correction can be much more easily implemented and understood in the SCTST-θ framework. In this case, the energy is effectively expanded to a fourth order polynomial in θ, where the first two coefficients are as determined by VPT2, and the third and fourth order coefficients are chosen such that the forward and reverse barrier heights are correct, and that the slope of $E(\theta)$ is zero at the reactant energy. An additional parameter $\theta_{\max}$, is required, which is equal to the barrier penetration integral at $E = 0$ This is calculated numerically

using Eq. 33, and the composite potential discussed previously.

$$\theta_{\max} = \sqrt{2m} \int \sqrt{V(y)} \mathrm{d}y \tag{33}$$

$E(\theta)$ is then given by:

$$\begin{aligned} E(n^{\ddagger}, \theta) =& \Delta V_f - \hbar \omega^*_{n_{\ddagger}} \frac{\theta}{\pi} - \hbar x_{FF} \left(\frac{\theta}{\pi} \right)^2 \\ &+ \left[3\omega^*_{n_{\ddagger}} \left(\frac{\theta_{\max}}{\pi} \right) + 2x_{FF} \left(\frac{\theta_{\max}}{\pi} \right)^2 - 4\Delta V_r \right] \left(\frac{\theta}{\theta_{\max}} \right)^3 \\ &- \left[2\omega^*_{n_{\ddagger}} \left(\frac{\theta_{\max}}{\pi} \right) + \quad x_{FF} \left(\frac{\theta_{\max}}{\pi} \right)^2 - 3\Delta V_r \right] \left(\frac{\theta}{\theta_{\max}} \right)^4, \end{aligned} \tag{34}$$

If an exothermic reaction were studied, then ΔV_r in the coefficient of the third and forth terms of θ should be replaced by ΔV_f. It is also interesting to note that this equation is akin to a VPT6 level expansion of energy, as it contains θ terms of the third and fourth orders. However, the coefficients of these terms in this equation are not derived from information at the TS, as one would have done in VPT6, instead they are chosen specifically to correct the energy threshold problem.[42]

3.2.1. Application of SCTST-θ

To illustrate the features of SCTST-θ discussed so far, we apply the various methods to the symmetric H-transfer reaction, CH_4+CH_3 in one-dimension. The *ab initio* calculations were performed at CCSD(T)//MP2/aug-cc-pVTZ level of theory. The VPT4 coefficients were determined from derivatives obtained from a sixth order polynomial function fitted to a total of 21 single point energies at the TS and the displaced geometries along the reaction coordinate. This method was able to reproduce previously calculated VPT2 coefficients[39] to good accuracy, as shown in Table. 1.

Fig. 6(a) shows how E_v varies as a function of θ for VPT2, VPT4 and Wagner's DT correction. Note that here, $E_{\text{thresh}} = 0$. Wagner's DT correction behaves correctly by

Table 1: VPT2 and VPT4 constants calculated using a fit to a sixth order polynomial, and as calculated previously using Richardson extrapolation. Values in cm^{-1}

	6th Order Polynomial	Richardson Extrapolation[39]	Difference
G	−81.645	−78.82	4%
X	−326.58	−315.36	4%
Y	−55.59	−	−

construction, however both the VPT2 and the VPT4 fail to produce $E_{\min} = 0$, the correct deep tunneling behaviour.

The 1D SCTST-θ rate constants calculated using these three methods are shown in Fig. 6(b). By comparison to results obtained from a 2D QRS calculation,[28] we can see that the DT corrected VPT2 rate constant has the best agreement to the QRS for the entire temperature range. Both VPT2 and VPT4 underestimate the reaction rate, especially at temperatures below 300K, where deep tunneling has a more significant contribution to the reaction. This result is in agreement with our prediction from the E_v *vs* θ plot in Fig. 6(a). It is also interesting to note that for this particular reaction the VPT4, having greater $E_{\min}$ than the VPT2, has a worse behaviour in the deep tunneling regime than the VPT2.

In previous studies,[43,44] VPT4 has been shown to improve behaviour in the deep tunneling regime, in contrast to what we observe here. In these works, only one-dimensional potentials were studied. Whilst our results suggest that VPT4 will improve the description of a one-dimensional, Eckart-like potential, this may not be true of a multidimensional, complex potential seen in real chemical systems. Accurately determining the threshold energy from derivatives at the TS requires substantial knowledge about the intermode couplings, since these couplings have a severe impact on the reaction path away from the TS. Thus one expects only a very high order of perturbation theory could correctly describe the deep tunneling regime. It is thus clear that the method of Wagner[42] is a more efficient way to ensure the behaviour is correct, without requiring detailed knowledge of these couplings. In fact a similar treatment can be implemented to the VPT4 calculation, in which case, terms

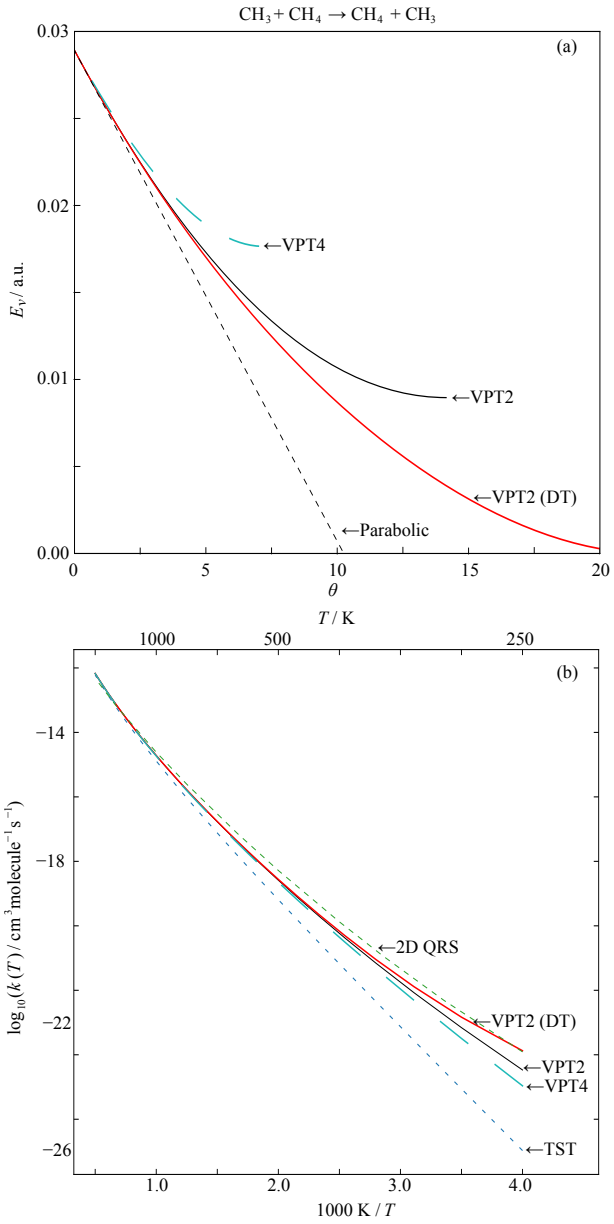

Figure 6: Application of 1D SCTST-θ to the $CH_3 + CH_4 \rightarrow CH_4 + CH_3$ reaction. (a) Plot of the VPT2, VPT4, and DT corrected E_v as a function of *theta* and (b) plot of calculated reaction rate constants compared to a 2D QRS result.[28]

of the fourth and fifth power of θ can be added to Eq. 32 to specifically correct the E_{min} so that $E_{\text{min}} = E_{\text{thresh}}$. This may lead to slightly more accurate results.

4. Application to complex systems

4.1. Internal Rotations

Internal rotational (or hindered rotational, HR) degrees of freedom must be treated carefully in any normal mode analysis. They behave as harmonic oscillators at low temperatures, but as free rotors in the high temperature limit - yet there is no simple analytical expression for their exact partition function. Moreover, internal rotations can lead to anomalous coupling terms in a FD-VPT2 treatment, a result of their motion being poorly described by Cartesian (as opposed to internal, curvilinear) coordinates. Their careful treatment is especially important for reactions in which an internal rotation is present in only one of the reactant or product states; in this case, there can be no cancellation of errors when the ratio of the partition function is taken in order to calculate the rate constant. Several approximate treatments for internal rotational DOFs have been suggested.[47–49] Here, we focus on simple one-dimensional treatments.

An initial assumption is that the HR is separable from the other degrees of freedom. This can be verified by observing a small change in normal mode frequencies when the internal rotor is projected out of the Hessian matrix, and is often found to be valid, owing to the significantly lower frequency internal rotors typically have.[39] This separation allows for the HR to be treated with a simple 1D partition function treatment.

Truhlar and coworkers[50] have suggested treating a 1D internal rotation by fitting the rotational energy potential to a cosine Fourier series, from which the partition function is given by a sum over the eigenvalues of the system. This 'eigenvalue summation' method

requires the 1D torsional PES.

Truhlar *et al.*[50] have also suggested an approximate 1D partition function that moves smoothly from the harmonic (low temperature) limit, to the free rotor (high temperature) limit. This is illustrated in Fig. 7 for the rotor in the $H_3C{-}H{-}CH_3$ transition state. No additional *ab initio* calculations are required. The effects of this treatment on a reactive system were tested by Burd *et al.*,[39] who showed that this provides a qualitative difference to the simple harmonic oscillator approximation, and gives excellent agreement with the eigenvalue summation method, as shown in Fig. 8 (a).

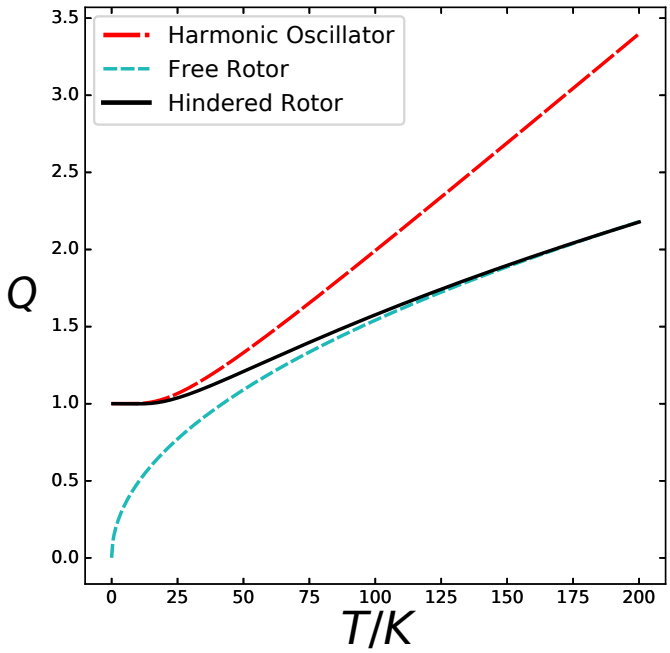

Figure 7: The 'tanh' approximation moves smoothly from the harmonic oscillator partition function at low temperature, to the free rotor partition function at high temperature. Here, parameters used were from the $H_3C{-}H{-}CH_3$ transition state rotor. It is clear the harmonic approximation is very poor above 100 K.

Accurate HR treatments are important even for reactions in which both reactant and transition state have internal rotational DOFs. The reaction of H with methanol in the gas phase has been the subject of extensive experimental and theoretical studies.[38,51–66] A recent

study[38] showed the harmonic approximation leads to significant errors, and worse agreement with experiment. This effect is shown in Fig. 8 (b).

Whilst the 1D solution to hindered rotor treatments is straightforward, their treatment in a FD-SCTST calculation less simple, as they cannot be treated as seperable from other degrees of freedom. A treatment by rectilinear (Cartesian) normal modes can lead to unphysically large couplings between it and other modes,[67,68] but a more sophisticated method, utilising curvilinear coordinates, is not currently routine. It is likely that more error is introduced by including a hindered rotor in a VPT2 calculation, than by projecting it out of the hessian matrix and treating it in one dimension. This leaves an (F-1) dimensional SCTST calculation.

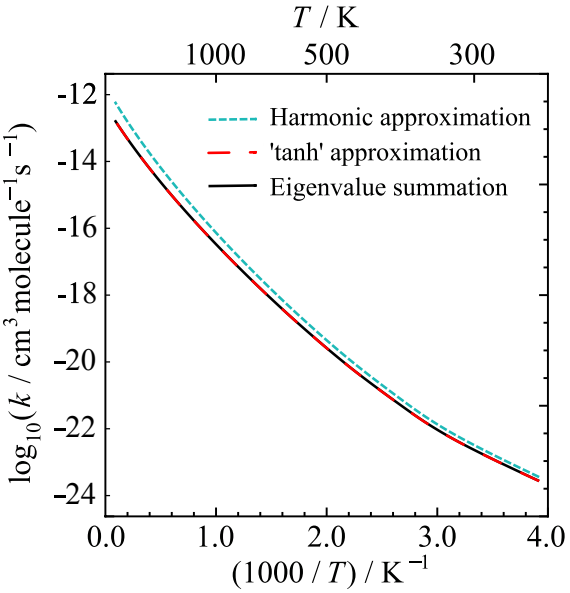

(a) $CH_3 + CH_4$ Reprinted with permission from Ref. 39

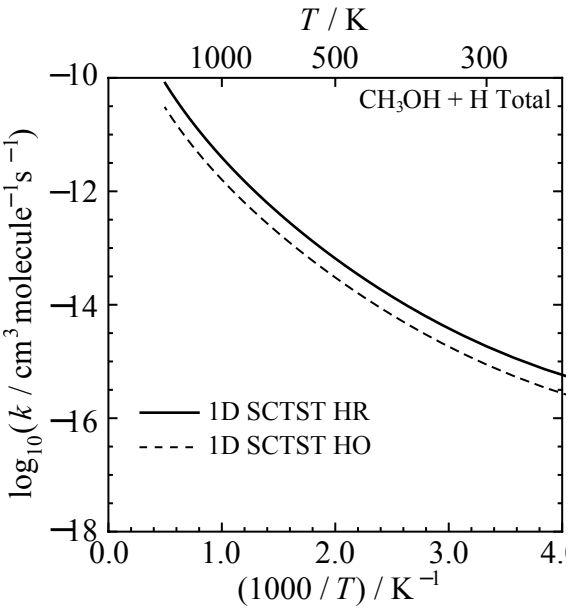

(b) $CH_3OH + H$

Figure 8: Rate constant comparisons using three treatments of the hindered rotor.

4.2. Application to degradation of nerve agents

Experimental studies on Chemical Warfare Agents (CWAs) can be difficult to accomplish due to the toxicity of the compounds and also must follow regulation under the Chemical Weapon Convention (CWC). Computational works on CWAs of course do not have the safety issues but face a different challenge, the size of the molecule.[40,69] For instance, in our recent study of reactions of the nerve agent VX with simulants, *O, S*-diethyl methylphosphonothiolate with 22 atoms (which is approximately half of the size of VX consisting of 42 atoms) has 7 internal rotation sites, 4 of which can produce conformational isomers. In this kind of situations, where multiple HR's are found in the system, approximate treatments to the HR partition function are available.[47,50,70,71] The most widely used method[47,70] is based on extending the 'tanh' approximation shown in Figs. 7 and 8 to a Boltzmann weighted multi-structural calculation. We recently showed how to implement these methods in SCTST calculations,[40,69] in particular to 1D SCTST. The 1D SCTST has a natural advantage in adapting these types of improvements on partition function calculations, since the tunneling correction in 1D SCTST is based on the potential energy profile along the reaction mode vibration, which is easily separated from the HR modes. Recently, in a combined theoretical and experimental study[40] of the thermodecomposition of the nerve agent sarin, 1D SCTST with multidimensional HR treatment was successfully applied. The calculated and measured survival percentage of sarin after 0.5 s of reaction time is presented in Fig. 9. The 1D SCTST shows excellent agreement to the experimental results. In addition, comparing to the TST results, we can see that even at relatively high temperature (between 600 and 775K as shown in the figure), quantum tunneling plays an important role in reaction dynamics.

4.3. Application to atmospheric reactions

Recent work in our group[41] studied the application of SCTST to the unimolecular decay of Criegee Intermediates (CIs). CIs play a significant role in atmospheric chemistry,[72,73] and their decay is thought to be a significant contributor to the OH budget in the atmosphere.[74]

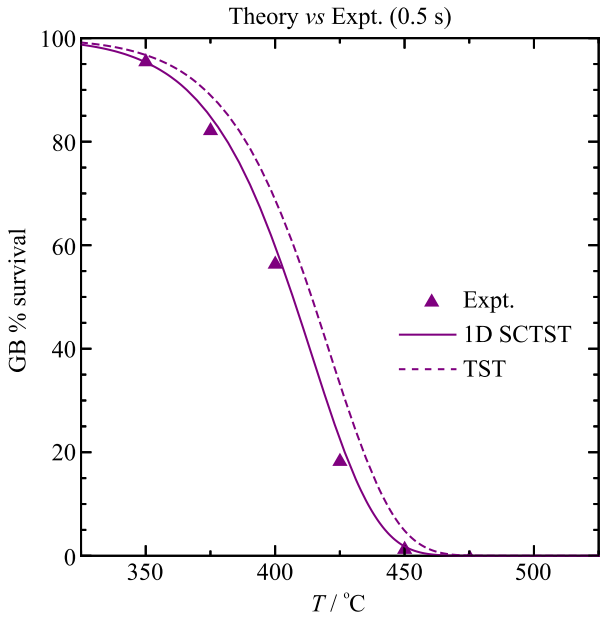

Figure 9: Plot of sarin percentage survival after 0.5 s reaction time vs temperature. Reprinted with permission from Ref. 40

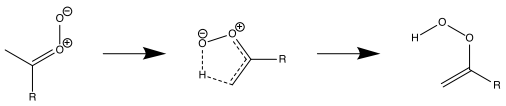

(a) 1,4 hydrogen transfer reaction

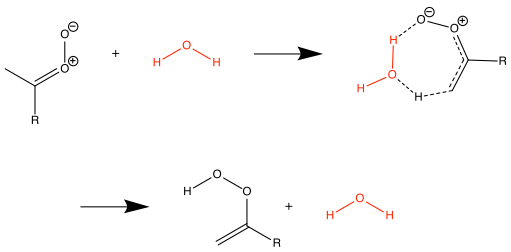

(b) One Water (Catalytic) - Same reaction as in (a), but with a single water molecule in the transition state, shown in red.

Figure 10: Unimolecular decay pathways of the Criegee intermediate.

As a result, the reactivity of these species has been the subject of extensive experimental and theoretical studies in recent years.[75–81]

CIs are typically formed in the atmosphere by the ozonolysis of alkene species. They can then react in a number of different ways, either bimolecularly with 'Criegee Scavengers'[79,82–86] or with other CI molecules,[87,88] or react unimolecularly.[89,90] One possible unimolecular decay, shown in Fig. 10 (a), is a key step in the generation of OH radicals, and so is of particular interest. This reaction can be catalysed by a single atmospheric water molecule, Fig. 10 (b), although the significance of this pathway under atmospheric conditions is not

well understood. The application of SCTST to this system provides insights not only into the atmospheric chemistry of CIs, but to the applicability of SCTST in reduced dimensions to the reactions of complex systems.

Thermal rate constants for the two processes shown in Fig. 10 were calculated using SCTST in full- and one-dimension, as described in detail by Ref. 41. Single point energy calculations were performed at the CCSD(T)//MP2/cc-pVTZ level of theory. For optimising transition states, a *tight* convergence criteria was used.

The results showed good agreement between 1D-, FD- and experimental rate constants for the uncatalysed process, as shown in Fig. 11. At 298 K, the 1D and FD rates differed by just 38 %. The addition of a water molecule to the transition state reduced the barrier height from 68 kJmol^{-1} to 33 kJmol^{-1}. In contrast to the uncatalysed reaction, the catalysed rate had significantly worse agreement between 1D and FD rates, differing by a factor of twelve at 200 K. In this case it is clear couplings between modes cannot be neglected.

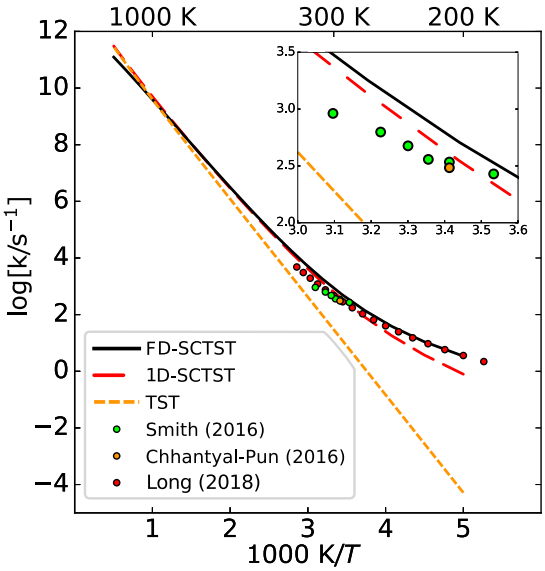

Figure 11: Results for the methylated, uncatalysed decomposition reaction. Comparison of experimental measurements (Chhantyal-Pun[91] and Smith[92]) and other theoretical results (Long)[93] with TST and SCTST in full and one dimensions (this work). The inset shows more clearly the comparison of this work to experiment. Reprinted with permission from Reference 41 (*Phys. Chem. Chem. Phys. 2018,20, 25224*).

Using the FD expression for x_{FF}, given in Section 2 in Eq. 18, in place of its one-dimensional approximation, can be used to incorporate some anharmonic effects in a cost effective way. The additional derivatives required can be obtained from the calculation of two Hessian matrices, displaced along the reaction coordinate This partially accounts for mode couplings, whilst maintaining the harmonic spectator mode treatment. The results, shown in Fig. 12 shows this clearly recovers a significant amount of the tunnelling, but discrepancies still remain. In the next section we discuss performing SCTST in higher dimensions, $1 < d < F$ to obtain FD quality results, with significantly less computational effort.

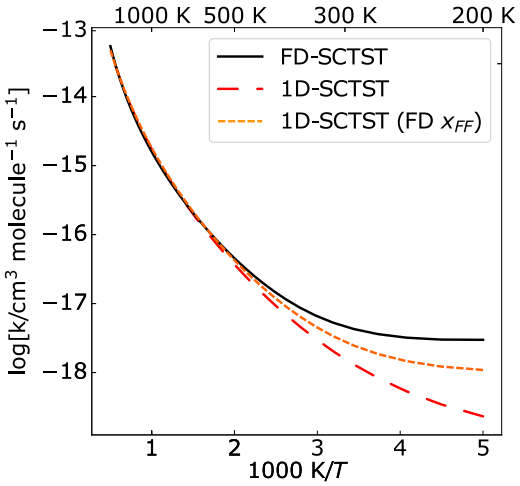

Figure 12: Comparison of FD-SCTST, 1D-SCTST and 1D-SCTST using the FD value of x_{FF} for the unmethylated, catalysed reaction. Reprinted with permission from Reference 41 (*Phys. Chem. Chem. Phys. 2018,20, 25224*).

4.4. RD SCTST

The contribution of each mode to the tunnelling process in the FD calculation can be investigated by studying the values of x_{iF}, as shown for the two Criegee transition states, in Fig. 13. These are calculated only in the FD treatment. It is clear that many of the spectator modes do not couple strongly to the reaction mode, and thus their inclusion in the FD model has little effect on the result. In particular, for the uncatalysed reaction, only one bound

mode is seen to interact strongly with the reaction mode. This suggests that whilst the 1D- model may be inadequate, the FD- model is inefficient as much computational time is spent calculating coupling constants that are close to zero. RD-SCTST seeks to bridge this gap, by treating some, but not all, of the bound modes anharmonically and coupled to the reaction mode. In this way, key couplings can be included, but no time is wasted including modes that are unimportant. RD-SCTST calculations are potentially much more efficient than FD-SCTST, as long as the significant modes can be identified in advance, cheaply. Here we will use the term RD- to refer to reduced dimensional methods other than 1D-SCTST.

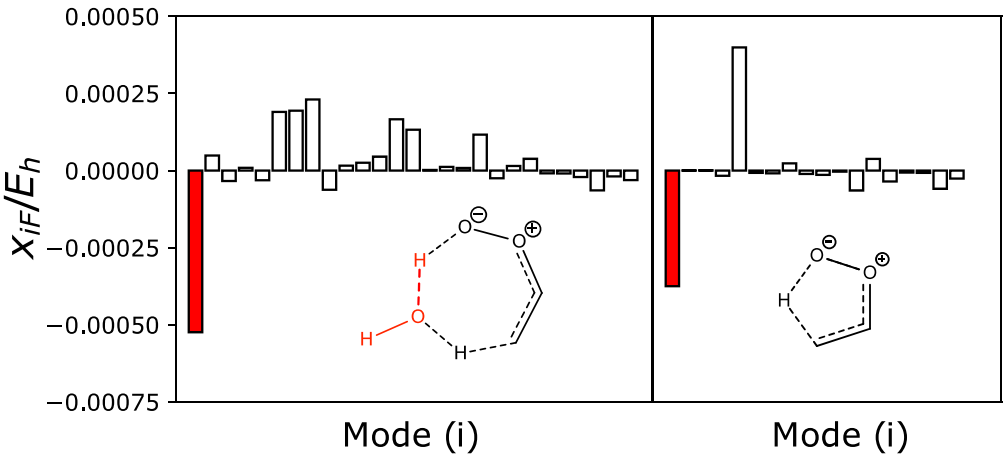

Figure 13: Comparison of values of x_{iF} for the catalysed and uncatalysed reaction. The reaction mode anharmonic constant (x_{FF}) is highlighted in red.

In principle, RD-SCTST can use any set of degrees of freedom as a basis to form the active space; previous studies have used a bond-breaking and bond-forming bond length basis to perform a two-dimensional calculation for simple hydrogen abstraction reactions.[17,24] In this work we use the transition state normal modes as the basis for the active degrees of freedom for simplicity; we will see this allows for straightforward identification of strongly coupled degrees of freedom, and can reduce the number of *ab initio* calculations required.

For a d-dimensional calculation, normal modes of the transition state can be divided into

d active modes and F-d spectator modes:

$$\nu = \left(\begin{array}{c} \nu_1 \\ \vdots \\ \nu_{F-d} \\ \nu_{F-d+1} \\ \vdots \\ \nu_F \end{array} \right) \begin{array}{l} \left. \begin{array}{c} \\ \\ \\ \end{array} \right\} \text{Spectator Modes} \\ \left. \begin{array}{c} \\ \\ \\ \end{array} \right\} \text{Active Modes} \end{array}$$

The active modes are comprised of the reaction mode, and the $d-1$ 'transition' modes. Spectator modes are treated harmonically, as in 1D-SCTST, and so only contribute to the rate through their partition function.

RD-SCTST presents two unique challenges - determining which modes are significant without calculation of the full anharmonic coupling matrix, $\mathbf{X}$, and ensuring a consistent anharmonic treatment of reactants and products. These are discussed in turn in the subsequent sections.

4.4.1. Selecting Active Modes

Unlike 1D or FD calculations, to perform an RD-SCTST calculation, special care must be taken to decide which, and how many, degrees of freedom to treat as active modes. A poor choice of active modes can lead to wasted computational effort, or introduction of errors that are fortuitously cancelled in a one-dimensional calculation. Adding in a single transition mode may also over compensate in one direction, and give a worse result than the one-dimensional calculation. This is illustrated in Fig. 14.

Thus we seek a cheap, automated method to estimate the coupling of each mode to the reaction mode using, for example, data available from a one-dimensional calculation. A

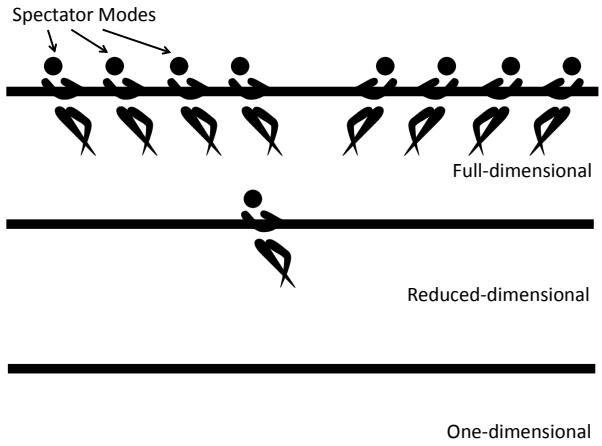

Figure 14: How reduced dimensionality calculations can go wrong, by comparison to modelling a tug-of-war. If the tug of war is close, the 1D model (with no players) is more accurate than the RD model (with one player pulling in one direction). In the same way, including some modes but not others in your calculation can give you the wrong answer. Here, the one-dimensional result is accurate due to a cancellation of errors in the full-dimensional calculation - this is lost in the two-dimensional calculation.

direct way to determine the significant couplings is to study the semi-diagonal fourth order derivatives, f_{FFii}, and third order derivatives of the form f_{Fij}, which are available from just two Hessians, at geometries displaced along the reaction coordinate, using a method similar to that of Barone:[31]

$$f_{FFii} = \frac{H_{ii}(\delta Q_F) + H_{ii}(-\delta Q_F) - 2H_{ii}(0)}{\delta Q_F^2} \tag{35}$$

and

$$f_{Fij} = \frac{H_{ij}(\delta Q_F) - H_{ij}(-\delta Q_F)}{2\delta Q_F} \tag{36}$$

where $H_{ij}(\delta Q)$ is element (i, j) of the Hessian matrix calculated at a geometry displaced from the transition state by a distance δQ. Note this calculation is significantly cheaper than calculating the $2F$ Hessians required for a FD calculation.

Using these, and the harmonic frequencies, x_{iF} can be approximated by x_{iF}^{approx}:

$$x_{iF}^{\text{approx}} = \frac{1}{4\omega_i\omega_F}\left(f_{iiFF} + \sum_{j=1}^{F} \frac{2f_{ijF}^2\left(\omega_i^2 + \omega_F^2 - \omega_j^2\right)}{\left[\left(\omega_i + \omega_F\right)^2 - \omega_j^2\right]\left[\left(\omega_i - \omega_F\right)^2 - \omega_j^2\right]}\right) \tag{37}$$

which serves as an approximation to the exact expression:

$$x_{iF} = \frac{1}{4\omega_i\omega_F}\left(f_{iiFF} - \sum_{j=1}^{F}\frac{f_{iij}f_{jFF}}{\omega_j^2} + \sum_{j=1}^{F}\frac{2f_{ijF}^2\left(\omega_i^2+\omega_F^2-\omega_j^2\right)}{\left[\left(\omega_i+\omega_F\right)^2-\omega_j^2\right]\left[\left(\omega_i-\omega_F\right)^2-\omega_j^2\right]}\right) \tag{38}$$

where the term in red is not present in x_{iF}^{approx}.

In Fig. 15, we show that an analysis of the transition states for the catalysed and uncatalysed Criegee decays, x_{iF}^{approx} provides an excellent approximation to x_{iF}, and clearly allows for the most significant modes to be distinguished.

Once the key modes have been identified, displaced Hessians along these modes are calculated, allowing for the full calculation of x_{ii} and x_{iF} terms, using derivatives calculated in the same way as in Eqs. 35 and 36. The anharmonic matrix can thus be constructed using Eq. 38 and:

$$x_{ii} = \frac{\hbar^2}{16\omega_i^2}\left(f_{iiii} - \sum_{j=1}^{i}\frac{f_{iij}^2}{\omega_j^2}\frac{8\omega_i^2-3\omega_j^2}{4\omega_i^2-\omega_j^2}\right) \tag{39}$$

As illustrated in Fig. 15, for the uncatalysed reaction, this procedure clearly identifies a single mode is significant ($\omega = 1875\text{cm}^{-1}$). For the catalysed reaction several modes are identified as significant ($\omega = 1745, 1633, 1264, 1650, 1203, 886\ \text{cm}^{-1}$).

4.4.2. Consistent Anharmonic Treatment

Once the significant modes have been determined, the way in which their anharmonicity is included must be considered. As the rate is calculated by taking the ratio of vibrational partition functions of the transition state and reactants, anharmonicity must be treated in an equivalent way in both systems in order to ensure the associated errors cancel as much as possible, as shown in Eq. 3 and Fig. 1(b).

The most rigorous way to perform an RD calculation is to isolate the $(F-d)$ spectator degrees of freedom through a curvilinear projection[28] in the TS, and their projection onto the reactant state. This leaves a system with d -degrees of freedom with which a d-dimensional

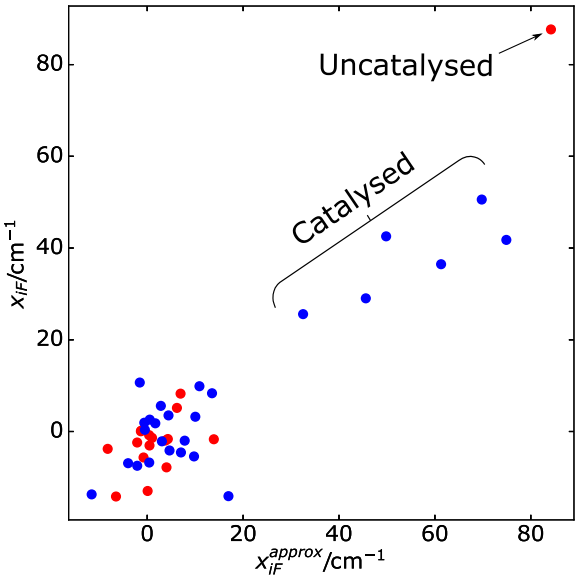

Figure 15: Using derivatives available from just two hessian calculations, x_{iF} can be approximated using Eq. 37. This allows the significant modes to be identified. Here, modes of the uncatalysed TS are in red, and modes of the catalysed TS are in blue.

SCTST calculation can be done in much the same way as a FD-SCTST calculation is done normally. This method does not limit RD calculations to using a normal mode basis, but could be implemented using, for example, a 'bond-breaking' and 'bond-forming' DOF basis for a 2D calculation.

Whilst theoretically rigorous, this method may be less convenient than others. It requires further Hessians to be calculated in the reactant state, in order to account for anharmonicity of the projected modes. Moreover, this becomes a less simple extension of 1D-SCTST, which is the desired outcome. The normal mode basis is also a convenient way to look at the reaction for when it is not clear *a priori* what degrees of freedom may be relevant. Choosing an orthogonal basis (unlike bond stretching bases) also allows for systematic inclusion of more modes, where each can build directly on the computation of the previous result.

When only a few modes are to be considered active ($d \ll F$) it is likely the error in treating these modes anharmonically in only the TS will be small. This is especially true in bimolecular reactions if the active modes partially or completely project onto degrees of

freedom in the reactant state which correspond to relative translational/rotational degrees of freedom (whose contribution to the vibrational partition function is zero). Such modes are illustrated in Fig. 16 for the $H_3C{-}H{-}CH_3$ transition state. In this work we have adopted this simplified approach.

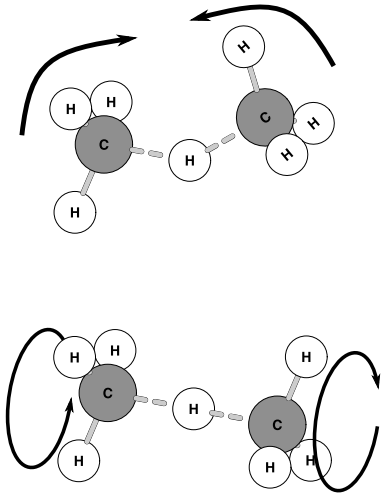

Figure 16: Some modes that correspond to relative translational and rotational modes in the reactant state.

4.4.3. Results

SCTST calculations were performed in RD for the two Criegee decay reactions using the modes determined as most significant by the method described in section 4.3.1. The results are shown in Fig. 17

From Fig. 17 (a) it is clear that adding in just a single bound mode gives a significant improvement to the rate. Whereas 1D SCTST is a factor of three smaller than the FD rate at 200K, the 2D calculation differs by just 40%. As expected, adding in the next most significant modes to the active space has only a small additional effect on the rate. For the catalysed reaction, multiple modes contribute significantly to the tunnelling process, and so a number of modes are required to achieve a similar accuracy to that of the uncatalysed reaction. The six-dimensional reaction lies within 30% of the FD rate at all temperatures evaluated.

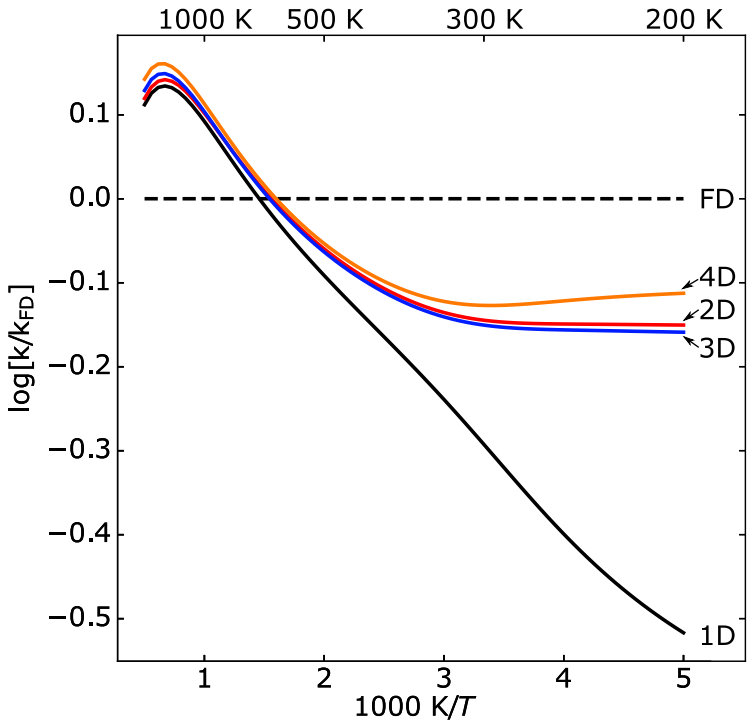

(a) Uncatalysed Criegee Reaction

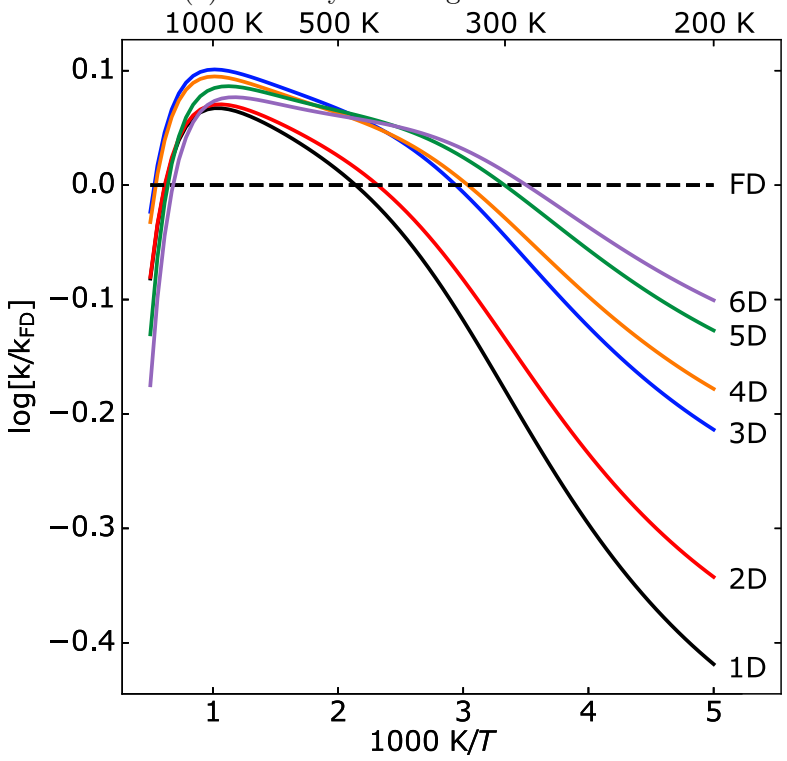

(b) Catalysed Criegee Reaction

Figure 17: Effect of including additional degrees of freedom in the tunneling calculations. The modes selected are those with the largest values of x_{iF}.

The development of RD-SCTST provides an extremely powerful tool for calculating SCTST rate constants in an efficient way, provided only a small number of bound modes interact. Further work is required to determine how common systems like this are.

4.5. Understanding corner-cutting included in SCTST

Semiclassical rate theories are able to simplify the calculation of rate constants for multi-dimensional reactions by defining distinct tunnelling pathways through which the reactive flux is calculated. The height and width of the pathway barrier very sensitively determines the tunnelling probability. The way in which these paths are determined from a multidimensional PES varies between methods. A simple choice of pathway is the minimum energy path (MEP) from the reactant to product configurations, as illustrated in Fig. 18 (a), which is easily determined from a steepest descent calculation from the TS. It is well known that tunnelling through the MEP often underestimates reaction probabilities due to neglecting corner-cutting effects. For reactions whose MEP exhibits large curvature, the reaction may dominantly proceed through a path with a higher, but narrower barrier, 'cutting the corner' of the MEP. This effect, known as 'corner-cutting', is most significant for 'heavy-light-heavy' type of reactions, in which a light atom is transferred between two heavy centres.

The effects of corner-cutting on the dynamics of chemical reactions has been studied extensively,[94–102] where a key challenge is determining the location on the PES of the important pathways.

Truhlar and coworkers have developed methods to incorporate multidimensional tunneling effects in variational Transition State Theory (VTST), accounting for corner-cutting effects. In the small-curvature tunnelling approximation (SCT), corner-cutting is accounted for by reducing the effective mass of the reaction coordinate, equivalent to shortening the tunneling path.[3,103,104] The new effective mass is determined from the reaction-path curvature. The large-curvature tunnelling (LCT) approximation[97,98,101,105,106] includes tunnelling

paths that are straight lines that connect the reactant and product wells, as illustrated in Fig. 18 (b). These paths can also connect configurations in different vibrational states. In microcannonically optimised tunnelling VTST (μOMT), the tunneling is calculated as the maximum of the SCT and LCT probabilities. Finally, the least-action tunneling model (LAT)[105,107] considers a large number of paths between the limits of the MEP and LCT paths.

Ring-polymer instanton rate theory[9,108] determines a single dominant tunnelling pathway by finding the path that represents a saddle point in the ring-polymer action, shown in Fig. 18 (c). The instanton can therefore be expected to accurately capture the corner cutting effects of the potential energy surface. Whilst this typically requires knowledge of a substantial part of the PES, recent advances, using machine learning methods, have reduced the number of *ab inito* calculations substantially.[109]

In this section we show that SCTST can be interpreted as a sum of 1D-SCTST rate constants, each corresponding to a different effective barrier height and width. These barriers can be associated with distinct corner-cutting trajectories, as illustrated in Fig. 18 (d). This interpretation gives a physical picture of how corner-cutting paths are incorporated into SCTST.

The connection between FD-SCTST, and individual 1D-SCTST paths is clear from comparing the key formulae for the rate. In 1D-SCTST, the action variable of the F^{th} degree of freedom can be written as a function of the Energy E_v, the barrier height ΔV_f and the barrier frequency ω_F:

$$\theta_{\text{1D}}(E_v, \Delta V_f, \omega_F) = \pi \frac{i\omega_F + \left[-\omega_F^2 + 4x_{FF}\left(\Delta V_f + G_0 - E_v\right)\right]^{1/2}}{2x_{FF}}. \tag{40}$$

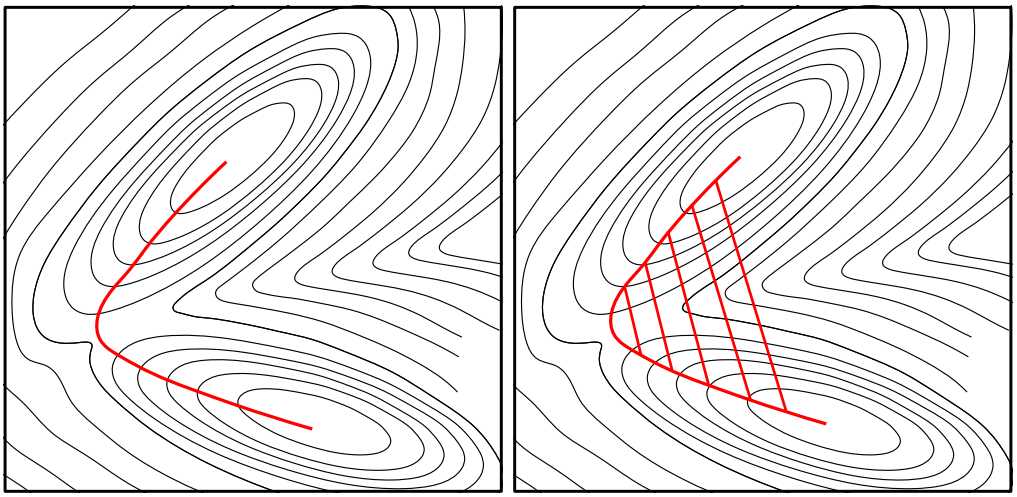

(a) Classical (minimum Energy Path)

(b) VTST + Large curvature Tunneling

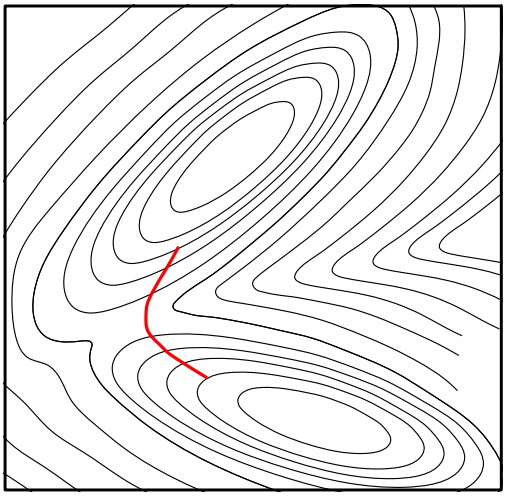

(c) Ring polymer Instanton

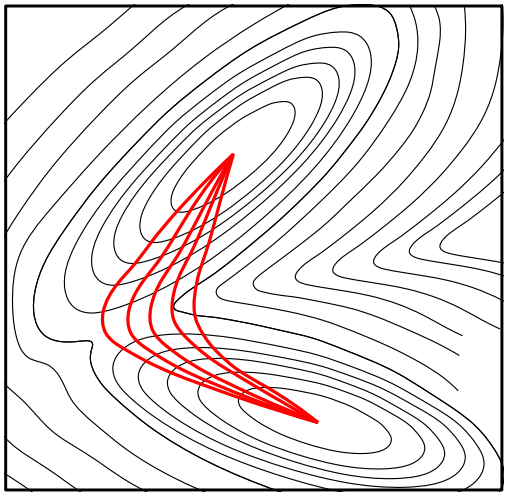

(d) SCTST

Figure 18: Illustration of how corner-cutting effects are accounted for in three semi-classical methods

In the case where the barrier height is replaced by an effective barrier,

$$V^{\text{eff}}_{\{n\}'} = \Delta V_f + E_{\{n\}'} \tag{41}$$

with

$$E_{\{n\}'} = \sum_{i=1}^{F} \hbar\omega_i \left(n_i + 0.5\right) + \sum_{i<j}^{F} x_{ij} \left(n_i + 0.5\right)\left(n_j + 0.5\right) + G_0 \tag{42}$$

and the frequency replaced with and effective frequency,

$$\omega^{\text{eff}}_{\{n\}'} = \omega_F + \sum_{i=1}^{F-1} x_{iF}(n_i + 0.5) \tag{43}$$

the FD expression for θ is returned:

$$\begin{aligned}\theta_{\text{1D}}(E_v, V^{\text{eff}}_{\{n\}'}, \omega^{\text{eff}}_{\{n\}'}) &= \pi \frac{-\Omega_{\{n\}'} + \left[\Omega^2_{\{n\}'} + 4x_{FF}\left(\Delta V_f + G_0 - E_{\{n\}'} - E_v\right)\right]^{1/2}}{2x_{FF}} \\ &= \theta_{FD}(E_v, \{n\}')\end{aligned} \tag{44}$$

The state-dependant reaction probability is then given by:

$$P_{\{n\}'}(E_v) = \left(1 + \exp\left[2\theta_{\text{1D}}(E_v, V^{\text{eff}}_{\{n\}'}, \omega^{\text{eff}}_{\{n\}'}\right]\right)^{-1} \tag{45}$$

and the cumulative reaction probability is given by the sum over all state-dependant reaction probabilities at the energy E_v:

$$N(E_v) = \sum_{\{n\}'} P_{\{n\}'}(E_v). \tag{46}$$

The FD rate can thus be interpreted as a sum over one-dimensional barriers, with an

effective barrier height and frequency given by equations 41 and 43:

$$k_{\mathrm{FD}} = \sum_{\{n\}'} k_{\mathrm{1D}}(V^{\mathrm{eff}}_{\{n\}'}, \omega^{\mathrm{eff}}_{\{n\}'}) \tag{47}$$

where Eq. 47 is equally applicable to thermal and microcannonical rate constants. Each effective barrier corresponds to a vibrational configuration of the transition state. As a mode's quantum number, n_i, increases, the effective barrier increases as described by Eq. 41. If $x_{iF} > 0$, the corresponding effective frequency will also increase, representing a narrower barrier. These distinct barriers can then be interpreted as corner cutting paths. This is illustrated in Fig. 19, where barriers for a harmonic system is compared to a strongly anharmonic system. In the harmonic case, $x_{iF} = 0$, multiple paths are still summed over, and each subsequent barrier is higher than the last, but no barrier narrowing is seen.

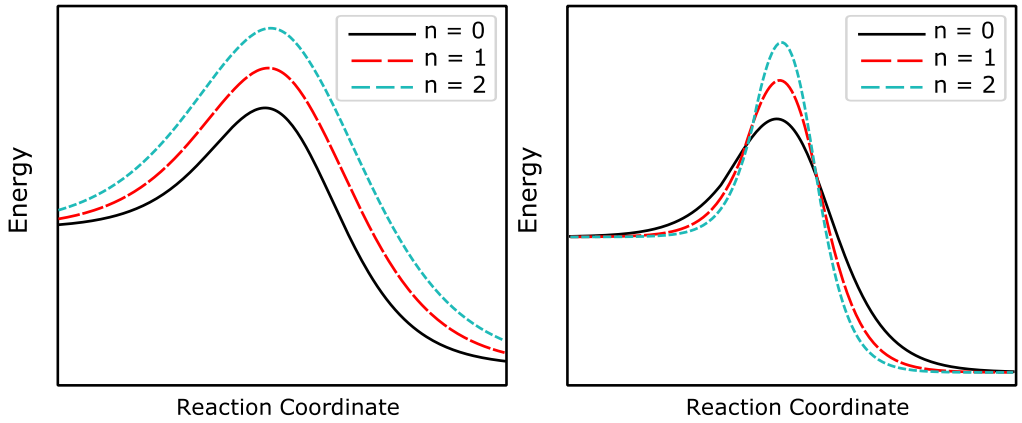

(a) Harmonic case (b) Significant Coupling

Figure 19: Illustrative paths for different active mode quantum numbers

It is interesting to ask whether these distinct pathways can be located on a given potential energy surface, in order to give insight about how the reaction proceeds. In general, this is only possible on a surface for which VPT2 is exact. In 1D, this corresponds to a harmonic oscillator, or a Morse potential. In multiple dimensions, however, the only simple potential for which VPT2 is exact is an uncoupled harmonic oscillator function. For anharmonic potentials, these paths do not exist on the 'real' PES, but rather on a 'pseudo-surface' for

which VPT2 is exact, and whose third and semi-diagonal fourth order derivatives match those of the 'real' surface.

5. Conclusion

Semiclassical Transition State Theory was first formulated in the 1970s by W. H. Miller and the first realistic applications of the theory were made by Miller and co-workers in the 1990s. However, it is only recently that the accuracy and power of this method for calculating tunneling effects on chemical reaction rate constants has been fully realised.

Comparisons with quantum reactive scattering calculations have demonstrated the accuracy of the method, even for reactions such as H atom transfer between two heavy molecules which have caused difficulties in the past. Furthermore the advances in quantum chemistry methods have allowed for the efficient and accurate calculation of the required quantities that are needed to apply the method - the second, third and fourth derivatives of the potential surface at the transition state of the reaction. In addition, the recent work has shown that only a small number of accurate *ab initio* computations are needed beyond those required in applications of regular transition state theory. The method also has the distinct advantage that a global potential energy surface does not need to be constructed.

This Feature Article has discussed some of the recent developments and applications of the SCTST performed in our own research group. In particular, we show that a reduced dimensional form of the SCTST is particularly efficient and reduces the required electronic structure calculations to an absolute minimum. We also describe how an alternative formulation of SCTST, called SCTST-θ, has advantages in allowing for straightforward applications of the SCTST for any form of the potential expansion at the transition state. When combined with a deep tunneling correction, which imposes the correct exothermicity or endothermicity on a reaction, this approach becomes particularly powerful.

We also describe some applications of the SCTST to more complex systems. Polyatomic

molecules often have many internal rotations and torsions and we examine computational procedures for dealing with these types of modes. We also describe some applications of the method to tunneling in unimolecular reactions. A particularly timely application of relevance to global security is to the degradation of chemical nerve agents, molecules which are very difficult to study in the laboratory. Another application described is the unimolecular decay of the atmospherically important Criegee intermediates which also occur through a hydrogen atom transfer via a cyclic transition state. Here it is also shown that a single water molecule significantly catalyses the reaction.

Using the Criegee intermediates as an example we also describe computational procedures for examining when the reduced dimensionality approach is most applicable and how to select the most active vibrational modes taking part in a chemical reaction. We also explain in some detail why the SCTST works so well for H atom exchange reactions of the heavy-light-heavy form where corner-cutting of the potential surface comes into play.

It has become clear that the SCTST is a very reliable and computationally inexpensive approach for treating quantum mechanical tunneling in chemical reactions. The method is a direct way of turning a minimal number of electronic structure calculations into rate constants. It is an important addition to the repertoire of *ab initio* methods that are enabling theory to make accurate and useful predictions on chemical reactions.

Acknowledgement

Helpful discussions with W. H. Miller on the SCTST-θ are gratefully acknowledged. X.S. acknowledges the use of the University of Oxford Advanced Research Computing facility in performing the theoretical studies in this work. X.S. and D.C.C. are thankful for the financial support of the Leverhulme Trust (Project Grant No. RPG-2013-321). X.S. and D.C.C. acknowledge support from DSTL CT&S R-Cloud Tender R100010-4370 and DSTL Grant No R1000121682. T. A. H. is grateful for support from the EPSRC Centre for Doctoral

Training in Theory and Modelling in Chemical Sciences (Project Grant No. EP/L015722/1).

References

(1) Suleimanov, Y. V.; Aoiz, F. J.; Guo, H. Chemical Reaction Rate Coefficients from Ring Polymer Molecular Dynamics: Theory and Practical Applications. *J. Phys. Chem. A* **2016**, *120*, 8488–8502.

(2) *Faraday Disucssions: Reaction Rate Theory*; Royal Society of Chemistry, 2016; Vol. 195.

(3) Bao, J. L.; Truhlar, D. G. Variational Transistion State Theory: Theoretical Framework and Recent Developments. *Chem. Soc. Rev.* **2017**, *46*, 7548–7596.

(4) Clary, D. C. Spiers Memorial Lecture Introductory Lecture: Quantum Dynamics of Chemcial Reactions. *Faraday Discuss.* **2018**, *212*, 9–32.

(5) Fu, B.; Shan, X.; Zhang, D. H.; Clary, D. C. Recent Advances in Quantum Scattering Calculations on Polyatomic Bimolecular Reactions. *Chem. Soc. Rev.* **2017**, *46*, 7625–7649.

(6) Zhao, B.; Guo, H. State-to-State Quantum Reactive Scattering in Four-Atom Systems. *WIREs Comput. Mol. Sci.* **2017**, *7*, e1301.

(7) Truhlar, D. G.; Garrett, B. C.; Klippenstein, S. J. Current Status of Transition-State Theory. *J. Phys. Chem.* **1996**, *100*, 12771–12800.

(8) Habershon, S.; Manolopoulos, D. E.; Markland, T. E.; Miller III, T. F. Ring-Polymer Molecular Dynamics: Quantum Effects in Chemical Dynamics from Classical Trajectories in an Extended Phase Space. *Ann. Rev. Phys. Chem.* **2013**, *64*, 387–413.

(9) Richardson, J. O. Ring-Polymer Instanton Theory. *Int. Rev. Phys. Chem.* **2018**, *37*, 171–216.

(10) Schlegel, H. B. Exploring Potential Energy Surfaces for Chemical Reactions: An Overview of Some Practical Methods. *J. Comput. Chem.* **2003**, *24*, 1514–1527.

(11) Qu, C.; Yu, Q.; Bowman, J. M. Permutationally Invariant Potential Energy Surfaces. *Annu. Rev. Phys. Chem.* **2018**, *69*, 151–175.

(12) Miller, W. H. Semiclassical Limit of Quantum Mechanical Transition State Theory for Nonseparable Systems. *J. Chem. Phys.* **1975**, *62*, 1899–1906.

(13) Miller, W. H. Semi-Classical Theory for Non-Separable Systems: Construction of "Good" Action-Angle Variables for Reaction Rate Constants. *Faraday Discuss. Chem. Soc.* **1977**, *62*, 40–46.

(14) Nguyen, T. L.; Stanton, J. F.; Barker, J. R. *Ab Initio* Reaction Rate Constants Computed Using Semiclassical Transition-State Theory: HO + H_2 → H_2O + H and Isotopologues. *J. Phys. Chem. A* **2011**, *115*, 5118–5126.

(15) Nguyen, T. L.; Stanton, J. F. High-Level Theoretical Study of the Reaction Beteween Hydroxyl and Ammonia: Accurate Rate Constants from 200 to 2500 K. *J. Chem. Phys.* **2017**, *147*, 152704.

(16) Greene, S. M.; Shan, X.; Clary, D. C. Quantum Scattering and Semiclassical Transition State Theory Calculations on Chemical Reactions of Polyatomic Molecules in Reduced Dimensions. *Adv. Chem. Phys.* **2018**, *163*, 117–149.

(17) Greene, S. M.; Shan, X.; Clary, D. C. Reduced-Dimensionality Semiclassical Transition State Theory: Application to Hydrogen Atom Abstraction and Exchange Reactions of Hydrocarbons. *J. Phys. Chem. A* **2015**, *119*, 12015–12027.

(18) Bowman, J. M. Reduced Dimensionality Theory of Quantum Reactive Scattering. *J. Phys. Chem.* **1991**, *95*, 4960–4968.

(19) Kerkeni, B.; Clary, D. C. *Ab Initio* Rate Constants from Hyperspherical Quantum Scattering: Application to H+CH_4 $\rightarrow$ H_2 + CH_3. *J. Chem. Phys.* **2004**, *120*, 2308–2318.

(20) Banks, S. T.; Clary, D. C. Chemcial Reaction Surface Vibrational Frequencies Evaluated in Curvilinear Internal Coordinates: Application to H + CH_4 $\rightleftharpoons$ H_2 + CH_3. *J. Chem. Phys.* **2009**, *130*, 024106.

(21) von Horsten, H. F.; Banks, S. T.; Clary, D. C. An Efficient Route to Thermal Rate Constants in Reduced Dimensional Quantum Scattering Simulations: Applications to the Abstraction of Hydrogen from Alkanes. *J. Chem. Phys.* **2011**, *135*, 094311.

(22) Shan, X.; Clary, D. C. Quantum Effects in the Abstraction Reaction by H Atoms of Primary and Secondary Hydrogens in n-C_4H_{10}: A Test of a New Potential Energy Surface Construction Method. *Phys. Chem. Chem. Phys.* **2013**, *15*, 1222–1231.

(23) Shan, X.; Clary, D. C. Qunatum Dynamics of the Abstraction Reaction of H with Cyclopropane. *J. Phys. Chem. A* **2014**, *118*, 10134–10143.

(24) Greene, S. M.; Shan, X.; Clary, D. C. An Investigation of One- Versus Two-Dimensional Semiclassical Transition State Theory for H Atom Abstraction and Exchange Reactions. *J. Chem. Phys.* **2016**, *144*, 084113.

(25) Miller, W. H. Recent Advances in Quantum Mechanical Reactive Scattering Theory, Including Comparison of Recent Experiments with Rigorous Calculations of State-to-State Cross Sections for the H/D+H_2 $\rightarrow$ H_2/HD + H Reactions. *Annu. Rev. Phys. Chem.* **1990**, *41*, 245–281.

(26) Miller, W. H.; Hernandez, R.; Handy, N. C.; Jayatilaka, D.; Willetts, A. *Ab Initio* Calculation of Anharmonic Constants for a Transition State, with Application to Semiclassical Transition State Tunneling Probabilities. *Chem. Phys. Lett.* **1990**, *172*, 62–68.

(27) Barker, J. R.; Nguyen, T. L.; Stanton, J. F. Kinetic Isotope Effects for Cl + CH_4 $\rightleftharpoons$ HCl + CH_3 Calculated Using *Ab Initio* Semiclassical Transition State Theory. *J. Phys. Chem. A* **2012**, *116*, 6408–6419.

(28) Banks, S. T.; Tautermann, C. S.; Remmert, S. M.; Clary, D. C. An Improved Treatment of Spectator Mode Vibrations in Reduced Dimensional Quantum Dynamics: Application to the Hydrogen Abstraction Reactions μ+CH_4, H+CH_4, D+CH_4, and CH_3+CH_4. *J. Chem. Phys.* **2009**, *131*, 044111.

(29) Meng, Q. Ring-Polymer Molecular Dynamics Study on Rate Coefficients of Hydrogen Abstraction of Methane: A Reduced-Dimensional Model. *Chem. Phys. Lett.* **2018**, *706*, 383–387.

(30) Beyer, A. N.; Richardson, J. O.; Knowles, P. J.; Rommel, J.; Althorpe, S. C. Quantum Tunneling Rates of Gas-Phase Reactions form On-the-Fly Instanton Calculations. *J. Phys. Chem. Lett.* **2016**, *7*, 4374.

(31) Barone, V. Anharmonic Vibrational Properties by a Fully Automated Second-Order Perturbative Approach. *J. Chem. Phys.* **2005**, *122*, 014108.

(32) Greene, S. M.; Shan, X.; Clary, D. C. Rate Constants of Chemical Reactions from Semiclassical Transition State Theory in Full and One Dimension. *J. Chem. Phys.* **2016**, *144*, 244116.

(33) Nguyen, T. L.; Barker, J. R. Sums and Densities of Fully Coupled Anharmonic Vibrational States: A Comparison of Three Practical Methods. *J. Phys. Chem. A* **2010**, *114*, 3718–3730.

(34) Wang, F.; Landau, D. P. Efficient, Multiple-Range Random Walk Algorithm to Calculate the Density of States. *Phys. Rev. Lett.* **2001**, *86*, 2050–2053.

(35) Wang, F.; Landau, D. P. Determining the Density of States for Classical Statistical Models: A Random Walk Algorithm to Produce a Flat Histogram. *Phys. Rev. E* **2001**, *64*, 056101.

(36) Basire, M.; Parneix, P.; Calvo, F. Quantum Anharmonic Densities of States Using the Wang-Landau Method. *J. Chem. Phys.* **2008**, *129*, 081101.

(37) Aieta, C.; Gabas, F.; Ceotto, M. An Efficient Computational Approach for the Calculation of the Vibrational Density of States. *J. Phys. Chem. A* **2016**, *120*, 4853–4862.

(38) Shan, X.; Clary, D. C. Application of One-Dimensional Semiclassical Transition State Theory to the $CH_3 + H \rightleftharpoons CH_2OH/CH_3O + H_2$ Reactions. *Phil. Trans. R. Soc. A* **2017**, *376*, 20170147.

(39) Burd, T. A. H.; Shan, X.; Clary, D. C. Tunnelling and the Kinetic Isotope Effect in $CH_3 + CH_4 \rightarrow CH_4 + CH_3$: An Application of Semiclassical Transition State Theory. *Chem. Phys. Lett.* **2018**, *693*, 88–94.

(40) Shan, X.; Vincent, J. C.; Kirkpatrick, S.; Walker, M. D.; Sambrook, M. R.; Clary, D. C. A Combined Theoretical and Experimental Study of Sarin (GB) Decomposition at High Temperatures. *J. Phys. Chem. A* **2017**, *121*, 6200–6210.

(41) Burd, T. A. H.; Shan, X.; Clary, D. C. Catalysis and Tunnelling in the Unimolecular Decay of Criegee Intermediates. *Phys. Chem. Chem. Phys.* **2018**, *20*, 25224.

(42) Wagner, A. F. Improved Multidimensional Semiclassical Tunneling Theory. *J. Phys. Chem. A* **2013**, *117*, 13089–13100.

(43) Stanton, J. F. Semiclassical Tranistion-State Theory Based on Fourth-Order Vibrational Perturbation Theory: The Symmetrical Eckart Barrier. *J. Phys. Chem. Lett.* **2016**, *7*, 2708–2713.

(44) Goel, P.; Stanton, J. F. Semiclassical Transition State Theory Based on Fourth Order Vibrational Perturbation Theory: Model System Studies beyond Symmetric Eckart Barrier. *J. Chem. Phys.* **2018**, *149*, 134109.

(45) Hernandez, R.; Miller, W. H. Semiclassical Transition State Theory: A New Perspective. *Chem. Phys. Lett.* **1993**, *214*, 129–136.

(46) Fermann, J. T.; Auerbach, S. Modeling Proton Mobility in Acidic Zeolite Clusters: II. Room Temperature Tunneling Effects from Semiclassical Rate Theory. *J. Chem. Phys.* **2000**, *112*, 6787.

(47) Ellingson, B. A.; Lynch, V. A.; Mielke, S. L.; Truhlar, D. G. Statistical Thermodynamics of Bond Torsional Modes: Tests of Separable, Almost-Separable, and Improved Pitzer-Gwinn Approximations. *J. Chem. Phys.* **2006**, *125*, 084305.

(48) Zheng, J.; Truhlar, D. G. Multi-Path Variational Transition State Theory for Chemical Reaction Rates of Complex Polyatomic Species: Ethanol + OH Reactions. *Faraday Discuss.* **2012**, *157*, 59–88.

(49) Lin, C. Y.; Izgorodina, E. I.; Coote, M. L. How Accurate Are Approximate Methods for Evaluating Partition Functions for Hindered Internal Rotations? *J. Phys. Chem. A* **2008**, *112*, 1956–1964.

(50) Chuang, Y.-Y.; Truhlar, D. G. Statistical Thermodynamics of Bond Torsional Modes. *J. Chem. Phys.* **2000**, *112*, 1221–1228.

(51) Blowers, P.; Ford, L.; Masel, R. *Ab Initio* Calculations of the Reactions of Hydrogen with Methanol: A Comparison of the Role of Bond Distortions and Pauli Repulsions on the Intrinsic Barriers for Chemical Reactions. *J. Phys. Chem. A* **1998**, *102*, 9267–9277.

(52) Kerkeni, B.; Clary, D. C. Kinetic Isotope Effects in the Reactions of D Atoms with CH_4, C_2H_6, and CH_3OH: Quantum Dynamics Calculations. *J. Phys. Chem. A* **2004**, *108*, 8966–8972.

(53) Cribb, P. H.; Dove, J. E.; Yamazaki, S. A Kinetic Study of the Pyrolysis of Methanol Using Shock Tube and Computer Simulation Techniques. *Combust. Flame* **1992**, *88*, 169–185.

(54) Lendvay, G.; Bérces, T.; Márta, F. An *ab Initio* Study of the Three-Channel Reaction between Methanol and Hydrogen Atoms: BAC-MP4 and Gaussian-2 Calculations. *J. Phys. Chem. A* **1997**, *101*, 1588–1594.

(55) Zhu, T.; Li, J.; Liotard, D. A.; Cramer, C. J.; Truhlar, D. G. Analytical Energy Gradients of a Self-Consistent Reaction-Field Solvation Model Based on CM2 Atomic Charges. *J. Chem. Phys.* **1999**, *110*, 5503–5513.

(56) Pu, J.; Ma, S.; Gao, J.; Truhlar, D. G. Small Temperature Dependence of the Kinetic Isotope Effect for the Hydride Transfer Reaction Catalyzed by *Escherichia coli* Dihydrofolate Reductase. *J. Phys. Chem. B* **2005**, *109*, 8551–8556.

(57) Tsang, W. Chemical Kinetic Data Base for Combustion Chemistry. Part 2. Methanol. *J. Phys. Chem. Ref. Data* **1987**, *16*, 471–508.

(58) Chuang, Y.-Y.; Truhlar, D. G. Nonequilibrium Solvation Effects for a Polyatomic Reaction in Solution. *J. Am. Chem. Soc.* **1999**, *121*, 10157–10167.

(59) Baulch, D. L.; Bowman, C. T.; Cobos, C. J.; Cox, R. A.; Just, T.; Kerr, J. A.; Pilling, M. J.; Stocker, D.; Troe, J.; Tsang, W. et al. Evaluated Kinetic Data for Combustion Modeling: Supplement II. *J. Phys. Chem. Ref. Data* **2005**, *34*, 757–1397.

(60) Li, S. C.; Williams, F. A. Experimental and Numerical Studies of Two-Stage Methanol Flames. *Symp. Combust.* **1996**, *26*, 1017–1024.

(61) Meana-Pañeda, R.; Truhlar, D. G.; Fernández-Ramos, A. High-Level Direct-Dynamics Variational Transition State Theory Calculations Including Multidimensional Tunneling of the Thermal Rate Constants, Branching Ratios, and Kinetic Isotope Effects of the Hydrogen Abstraction Reactions from Methanol by Atomic Hydrogen. *J. Chem. Phys.* **2011**, *134*, 094302.

(62) Meagher, J. F.; Kim, P.; Lee, J. H.; Timmons, R. B. Kinetic Isotope Effects in the Reactions of Hydrogen and Deuterium Atoms with Dimethyl Ether and Methanol. *J. Phys. Chem.* **1974**, *78*, 2650–2657.

(63) Aronowitz, D.; Naegeli, D. W.; Glassman, I. Kinetics of the Pyrolysis of Methanol. *J. Phys. Chem.* **1977**, *81*, 2555–2559.

(64) Hoyermann, K.; Sievert, R.; Wagner, H. G. Mechanism of the Reaction of H Atoms with Methanol. *Berichte der Bunsengesellschaft für Phys. Chemie* **1981**, *85*, 149–153.

(65) Carvalho, E. F. V.; Barauna, A. N.; Machado, F. B. C.; Roberto-Neto, O. Theoretical Calculations of Energetics, Structures, and Rate Constants for the $H + CH_3OH$ Hydrogen Abstraction Reactions. *Chem. Phys. Lett.* **2008**, *463*, 33–37.

(66) Jodkowski, J. T.; Rayez, M.-T.; Rayez, J.-C.; Bérces, T.; Dóbé, S. Theoretical Study of the Kinetics of the Hydrogen Abstraction from Methanol. 3. Reaction of Methanol with Hydrogen Atom, Methyl, and Hydroxyl Radicals. *J. Phys. Chem. A* **1999**, *103*, 3750–3765.

(67) Miller, W. H. Quantum Dynamics of Complex Molecular Systems. *Proc. Natl. Acad. Sci. U. S. A.* **2005**, *102*, 6660–6664.

(68) Jung, J. O.; Gerber, R. B. Vibrational Wave Functions and Spectroscopy of $(H_2O)_n$, n=2,3,4,5: Vibrational Self-Consistent Field with Correlation Corrections. *J. Chem. Phys.* **1996**, *105*, 10332–10348.

(69) Shan, X.; Sambrook, M. R.; Clary, D. C. Theoretical Study of Gas-Phase Unimolecular Decomposition of Simulants of the Nerve Agent VX. *J. Phys. Chem. A* **2019**, *123*, 59–72.

(70) Zheng, J.; Truhlar, D. G. Kinetics of Hydrogen-Transfer Isomerizations of Butoxyl Radicals. *Phys. Chem. Chem. Phys.* **2010**, *12*, 7782–7793.

(71) Zheng, J.; Yu, T.; Papajak, E.; Alecu, I. M.; Mielke, S. L.; Truhlar, D. G. Practical Methods for Including Torsional Anharmonicity in Thermochemical Calculations on Complex Molecules: The Internal-Coordinate Multi-Structural Approximation. *Phys. Chem. Chem. Phys.* **2011**, *13*, 10885–10907.

(72) Johnson, D.; Marston, G. The Gas-Phase Ozonolysis of Unsaturated Volatile Organic Compounds in the Troposphere. *Chem. Soc. Rev.* **2008**, *37*, 699–716.

(73) Kroll, J. H.; Sahay, S. R.; Anderson, J. G.; Demerjian, K. L.; Donahue, N. M. Mechanism of HO_x Formation in the Gas-Phase Ozone-Alkene Reaction. 2. Prompt versus Thermal Dissociation of Carbonyl Oxides to Form OH. *J. Phys. Chem. A* **2001**, *105*, 4446–4457.

(74) Harrison, R. M.; Yin, J.; Tilling, R. M.; Cai, X.; Seakins, P. W.; Hopkins, J. R.; Lansley, D. L.; Lewis, A. C.; Hunter, M. C.; Heard, D. E. et al. Measurement and Modelling of Air Pollution and Atmospheric Chemistry in the U.K. West Midlands Conurbation: Overview of the PUMA Consortium Project. *Sci. Total Environ.* **2006**, *360*, 5–25.

(75) Yin, C.; Takahashi, K. How Does Substitution Affect the Unimolecular Reaction Rates of Criegee Intermediates? *Phys. Chem. Chem. Phys.* **2017**, *19*, 12075–12084.

(76) Kuwata, K. T.; Luu, L.; Weberg, A. B.; Huang, K.; Parsons, A. J.; Peebles, L. A.; Rackstraw, N. B.; Kim, M. J. Quantum Chemical and Statistical Rate Theory Studies

of the Vinyl Hydroperoxides Formed in trans-2-Butene and 2,3-Dimethyl-2-butene Ozonolysis. *J. Phys. Chem. A* **2018**, *122*, 2485–2502.

(77) Huang, H.-L.; Chao, W.; Lin, J. J.-M. Kinetics of a Criegee Intermediate That Would Survive High Humidity and May Oxidize Atmospheric SO_2. *Proc. Natl. Acad. Sci. U. S. A.* **2015**, *112*, 10857–10862.

(78) Kumar, M.; Busch, D. H.; Subramaniam, B.; Thompson, W. H. Barrierless Tautomerization of Criegee Intermediates via Acid Catalysis. *Phys. Chem. Chem. Phys.* **2014**, *16*, 22968–22973.

(79) Berndt, T.; Voigtländer, J.; Stratmann, F.; Junninen, H.; Mauldin III, R. L.; Sipilä, M.; Kulmala, M.; Herrmann, H. Competing Atmospheric Reactions of CH_2OO with SO_2 and Water Vapour. *Phys. Chem. Chem. Phys.* **2014**, *16*, 19130–19136.

(80) Chao, W.; Hsieh, J.-T.; Chang, C.-H.; Lin, J. J.-M. Direct Kinetic Measurement of the Reaction of the Simplest Criegee Intermediate with Water Vapor. *Science* **2015**, *347*, 751–754.

(81) Vereecken, L.; Novelli, A.; Taraborrelli, D. Unimolecular Decay Strongly Limits the Atmospheric Impact of Criegee Intermediates. *Phys. Chem. Chem. Phys.* **2017**, *19*, 31599–31612.

(82) Lee, Y.-P. Perspective: Spectroscopy and Kinetics of Small Gaseous Criegee Intermediates. *J. Chem. Phys.* **2015**, *143*, 020901.

(83) Lewis, T. R.; Blitz, M. A.; Heard, D. E.; Seakins, P. W. Direct Evidence for a Substantive Reaction between the Criegee Intermediate, CH_2OO, and the Water Vapour Dimer. *Phys. Chem. Chem. Phys.* **2015**, *17*, 4859–4863.

(84) Smith, M. C.; Chang, C.-H.; Chao, W.; Lin, L.-C.; Takahashi, K.; Boering, K. A.; Lin, J. J.-M. Strong Negative Temperature Dependence of the Simplest Criegee In-

termediate CH_2OO Reaction with Water Dimer. *J. Phys. Chem. Lett.* **2015**, *6*, 2708–2713.

(85) Taatjes, C. A.; Welz, O.; Eskola, A. J.; Savee, J. D.; Scheer, A. M.; Shallcross, D. E.; Rotavera, B.; Lee, E. P. F.; Dyke, J. M.; Mok, D. K. W. et al. Direct Measurements of Conformer-Dependent Reactivity of the Criegee Intermediate CH_3CHOO. *Science* **2013**, *340*, 177–180.

(86) Chhantyal-Pun, R.; Davey, A.; Shallcross, D. E.; Percival, C. J.; Orr-Ewing, A. J. A Kinetic Study of the CH_2OO Criegee Intermediate Self-Reaction, Reaction with SO_2 and Unimolecular Reaction Using Cavity Ring-Down Spectroscopy. *Phys. Chem. Chem. Phys.* **2015**, *17*, 3617–3626.

(87) Buras, Z. J.; Elsamra, R. M. I.; Green, W. H. Direct Determination of the Simplest Criegee Intermediate (CH_2OO) Self Reaction Rate. *J. Phys. Chem. Lett.* **2014**, *5*, 2224–2228.

(88) Su, Y.-T.; Lin, H.-Y.; Putikam, R.; Matsui, H.; Lin, M. C.; Lee, Y.-P. Extremely Rapid Self-Reaction of the Simplest Criegee Intermediate CH_2OO and Its Implications in Atmospheric Chemistry. *Nat. Chem.* **2014**, *6*, 477–483.

(89) Womack, C. C.; Martin-Drumel, M.-A.; Brown, G. G.; Field, R. W.; McCarthy, M. C. Observation of the Simplest Criegee Intermediate CH_2OO in the Gas-Phase Ozonolysis of Ethylene. *Sci. Adv.* **2015**, *1*, e1400105.

(90) Fang, Y.; Liu, F.; Barber, V. P.; Klippenstein, S. J.; McCoy, A. B.; Lester, M. I. Deep Tunneling in the Unimolecular Decay of CH_3CHOO Criegee Intermediates to OH Radical Products. *J. Chem. Phys.* **2016**, *145*, 234308.

(91) Chhantyal-Pun, R.; Welz, O.; Savee, J. D.; Eskola, A. J.; Lee, E. P. F.; Blacker, L.; Hill, H. R.; Ashcroft, M.; Khan, M. A. H.; Lloyd-Jones, G. C. et al. Direct Measure-

ments of Unimolecular and Bimolecular Reaction Kinetics of the Criegee Intermediate $(CH_3)_2COO$. *J. Phys. Chem. A* **2017**, *121*, 4–15.

(92) Smith, M. C.; Chao, W.; Takahashi, K.; Boering, K. A.; Lin, J. J.-M. Unimolecular Decomposition Rate of the Criegee Intermediate $(CH_3)_2COO$ Measured Directly with UV Absorption Spectroscopy. *J. Phys. Chem. A* **2016**, *120*, 4789–4798.

(93) Long, B.; Bao, J. L.; Truhlar, D. G. Unimolecular Reaction of Acetone Oxide and Its Reaction with Water in the Atmosphere. *Proc. Natl. Acad. Sci. U. S. A.* **2018**, 201804453.

(94) Skodje, R. T.; Truhlar, D. G.; Garrett, B. C. Vibrationally Adiabatic Models for Reactive Tunneling. *J. Chem. Phys.* **1982**, *77*, 5955–5976.

(95) Tautermann, C. S.; Voegele, A. F.; Loerting, T.; Kohl, I.; Hallbrucker, A.; Mayer, E.; Liedl, K. R. Towards the Experimental Decomposition Rate of Carbonic Acid (H_2CO_3) in Aqueous Solution. *Chem. A Eur. J.* **2002**, *8*, 66–73.

(96) Skodje, R. T.; Truhlar, D. G.; Garrett, B. C. A General Small-Curvature Approximation for Transition-State-Theory Transmission Coefficients. *J. Phys. Chem.* **1981**, *85*, 3019–3023.

(97) Garrett, B. C.; Joseph, T.; Truong, T. N.; Truhlar, D. G. Application of the Large-Curvature Tunneling Approximation to Polyatomic Molecules: Abstraction of H or D by Methyl Radical. *Chem. Phys.* **1989**, *136*, 271–293.

(98) Fernandez-Ramos, A.; Truhlar, D. G. Improved Algorithm for Corner-Cutting Tunneling Calculations. *J. Chem. Phys.* **2001**, *114*, 1491–1496.

(99) Meana-Pañeda, R.; Truhlar, D. G.; Fernández-Ramos, A. Direct Dynamics Implementation of the Least-Action Tunneling Transmission Coefficient. Application to the

$CH_4/CD_3H/CD_4$ + CF_3 Abstraction Reactions. *J. Chem. Theory Comput.* **2010**, *6*, 3015–3025.

(100) Marcus, R. A.; Coltrin, M. E. A New Tunneling Path for Reactions Such as $H + H_2 \rightarrow H_2 + H$. *J. Chem. Phys.* **1977**, *67*, 2609–2613.

(101) Bondi, D. K.; Connor, J. N. L.; Garrett, B. C.; Truhlar, D. G. Test of Variational Transition State Theory with a Large Curvature Tunneling Approximation against Accurate Quantal Reaction Probabilities and Rate Coefficients for Three Collinear Reactions with Large Reaction Path Curvature: Cl+HCl, Cl+DCl, and Cl+MuCl. *J. Chem. Phys.* **1983**, *78*, 5981–5989.

(102) Fernandez-Ramos, A.; Zgierski, M. Z. Theoretical Study of the Rate Constants and Kinetic Isotope Effects of the 1,2-Hydrogen-Atom Shift of Methoxyl and Benzyloxyl Radicals Assisted by Water. *J. Phys. Chem. A* **2002**, *106*, 10578–10583.

(103) Liu, Y. P.; Lynch, G. C.; Truong, T. N.; Lu, D. H.; Truhlar, D. G.; Garrett, B. C. Molecular Modeling of the Kinetic Isotope Effect for the [1,5]-Sigmatropic Rearrangement of cis-1,3-Pentadiene. *J. Am. Chem. Soc.* **1993**, *115*, 2408–2415.

(104) Lu, D.-H.; Truong, T. N.; Melissas, V. S.; Lynch, G. C.; Liu, Y.-P.; Garrett, B. C.; Steckler, R.; Isaacson, A. D.; Rai, S. N.; Hancock, G. C. et al. POLYRATE 4: A New Version of a Computer Program for the Calculation of Chemical Reaction Rates for Polyatomics. *Comput. Phys. Commun.* **1992**, *71*, 235–262.

(105) Garrett, B. C.; Truhlar, D. G. A Least-Action Variational Method for Calculating Multidimensional Tunneling Probabilities for Chemical Reactions. *J. Chem. Phys.* **1983**, *79*, 4931–4938.

(106) Garrett, B. C.; Abusalbi, N.; Kouri, D. J.; Truhlar, D. G. Test of Variational Transition State Theory and the Least-Action Approximation for Multidimensional Tunnel-

ing Probabilities against Accurate Quantal Rate Constants for a Collinear Reaction Involving Tunneling into an Excited State. *J. Chem. Phys.* **1985**, *83*, 2252–2258.

(107) Kreevoy, M. M.; Ostovic, D.; Truhlar, D. G.; Garrett, B. C. Phenomenological Manifestations of Large-Curvature Tunneling in Hydride-Transfer Reactions. *J. Phys. Chem.* **1986**, *90*, 3766–3774.

(108) Richardson, J. O. Microcanonical and Thermal Instanton Rate Theory for Chemical Reactions at All Temperatures. *Faraday Discuss.* **2016**, *195*, 49–67.

(109) Laude, G.; Calderini, D.; Tew, D. P.; Richardson, J. O. *Ab Initio* Instanton Rate Theory Made Efficient Using Gaussian Process Regression. *Faraday Discuss.* **2018**, *212*, 237–258.

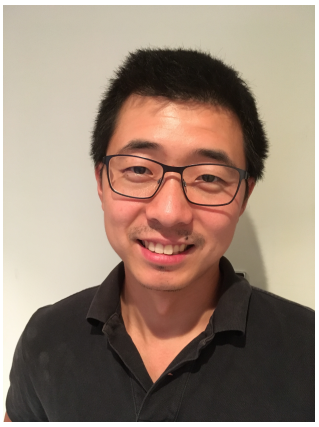

Xiao Shan undertook his PhD (2006-2010) at the University of Manchester with Professor J. N. L. Connor. He has worked as a postdoctoral research associate in Professor D. C. Clary's group in the Chemistry Department at the University of Oxford since 2011. His main research interest is in application of quantum and semiclassical methods to chemical reactions involving typically more than 10 atoms, and in numerical analyses to differential cross-sections of reactive scattering process.

Tim Burd joined the Department of Chemistry at the University of Oxford in 2016, and he is currently pursuing a DPhil degree in theoretical chemistry under the supervision of Prof. Sir David Clary. His research focuses on the development of efficient rate theories for studying a wide range of chemical systems. He is also the co-host of the chemistry podcast 'Theoretically Speaking'.

David Clary has been President of Magdalen College Oxford since 2005. He also directs a research group in the Chemistry Department at Oxford University working on the quantum theory of chemical reactions. He was the first Chief Scientific Advisor to the UK Foreign and Commonwealth Office (2009-2013) and was President of the Faraday Division of the Royal Society of Chemistry (2006-9). He was elected as a Fellow of the Royal Society in 1997 and was knighted by the Queen for services to international science in 2016.

Graphical TOC Entry